Intratumoral Tcf1^{+} PD1^{+} CD8 T cells with stem-like properties promote tumor control in response to vaccination and checkpoint blockade immunotherapy

Imran Siddiqui[1], Karin Schaeuble[1], Vijaykumar Chennupati[1,6], Silvia A. Fuertes Marraco[1], Sandra Calderon-Copete[2], Daniela Pais Ferreira[1], Santiago J. Carmona[1,3,4], Leonardo Scarpellino[5], David Gfeller[1,3,4], Sylvain Pradervand[2], Sanjiv A. Luther[5], Daniel E. Speiser[1] and Werner Held[1,7 *]

[1] Department of Oncology UNIL CHUV, University of Lausanne, 1066 Epalinges, Switzerland

[2] Lausanne Genomic Technologies Facility (LGTF), University of Lausanne, 1015 Lausanne, Switzerland

[3] Ludwig Institute for Cancer Research, University of Lausanne, 1066 Epalinges, Switzerland

[4] Swiss Institute of Bioinformatics (SIB), 1015 Lausanne, Switzerland

[5] Department of Biochemistry, University of Lausanne, 1066 Epalinges, Switzerland

[6] Present address: Discovery Biology Division, Syngene International Ltd, 560056 Bengaluru, India

[7] Lead contact

* Correspondence to: Werner.Held@unil.ch

SUMMARY

Immune checkpoint blockade can restore T cell-mediated immune responses and lead to striking and sustained clinical tumor regression. However, since chronic T cell activation promotes an epigenetically regulated, terminal T cell differentiation program, commonly termed exhaustion, it has remained unclear how checkpoint blockade mediates a proliferative response of tumor infiltrating T cells. Here, we identified human and murine intratumoral CD8 T cells expressing Tcf1 (T cell factor 1), which combine hallmarks of exhausted cells, including the expression of the checkpoint protein PD1 (Programmed Death 1) and key properties of central memory T cells. Preclinical mouse models reveal that sustained tumor control in response to checkpoint blockade or therapeutic vaccination critically depends on intratumoral $Tcf1^{+}$ $PD1^{+}$ CD8 T cells, that have the capacity to self-renew and generate an expanded pool of differentiated $Tcf1^{-}$ $PD1^{+}$ T cells. Tumors thus harbor stem-like CD8 T cells whose therapeutic targeting promotes immune control of cancer.

INTRODUCTION

The extent of CD8 T cell infiltration into certain tumors is predictive of overall patient survival, indicating that lymphocytes can restrict tumor outgrowth. Notwithstanding most infiltrated tumors progress suggesting that spontaneous anti-tumor immune responses are usually insufficient to control tumors. Immunotherapy aims at boosting anti-tumor immune responses to induce durable tumor control. Current approaches include adoptive cell therapy of autologous T cells and the blockade of inhibitory receptors ("immune checkpoints") yielding unprecedented clinical benefit in several tumor types (Rosenberg and Restifo, 2015) (Ribas and Wolchok, 2018) (Spranger and Gajewski, 2018). Clinical responses correlate with preexisting $CD8^+$ T cell infiltration and the neoantigen burden (Tumeh et al., 2014) (Schumacher and Schreiber, 2015). Advances in cancer genomics and proteomics have revolutionized the discovery of such tumor neoantigens that are usually unique to individual patients (Schumacher and Schreiber, 2015). Personalized therapeutic vaccination against neoantigens may thus provide an additional approach for effective immune therapy. Indeed, therapeutic vaccination can be as effective as checkpoint blockade in preclinical mouse models (Gubin et al., 2014). However, since T cell responses to neoantigens as well as tumor-associated antigens are compromised (Baitsch et al., 2011; Gros et al., 2014) it has remained unclear how therapeutic vaccination or checkpoint blockade improves the T cell response to tumors.

Persistent exposure to cognate antigen due to progressively growing tumors or chronic viral infection promotes an epigenetic T cell differentiation program that severely limits effector functions, alters the metabolic fitness and induces negative regulators of T cell function such as the co-inhibitory receptor PD1 (programmed cell death protein 1) (Wherry and Kurachi, 2015). This exhausted phenotype is generally thought to describe terminally differentiated cells that have lost expansion capacity and may be short-lived. However the notion of terminal differentiation is difficult to reconcile with the proliferation of intratumoral CD8 T cells in response to PD1 blockade (Tumeh et al., 2014). In addition, tumor-derived T cells expanded *in vitro* can mediate therapeutic responses following adoptive transfer (Rosenberg and Restifo, 2015), indicating that tumor-reactive T cells are not terminally differentiated or that at least some of these cells are not terminally differentiated (Speiser et al., 2014).

Tumor infiltrating CD8 T cells show significant heterogeneity both in cancer patients and experimental models (Reiser and Banerjee, 2016), which has been confirmed and considerably extended using single cell RNAseq analyses (Tirosh et al., 2016) (Singer et al., 2016) (Wei et al., 2017). However the functional relevance of the different subsets has remained unclear as the specificity of CD8 T cells

was not known and a considerable fraction of infiltrating CD8 T cells are bystanders (Simoni et al., 2018). Further, the diversity of CD8 T cells may originate from cells initially present in the blood or other tissues or may derive from intratumor turn over. Consequently, the source and the clonal relationship of intratumoral CD8 T cell subsets remains poorly understood.

Similar to tumors, chronic viral infections promote T cell exhaustion and this has been thought to preclude the formation of memory. However, a subset of virus-specific CD8 T cells co-expressing the central memory transcription factor T cell factor 1 (Tcf1, encoded by the *Tcf7* gene) (Jeannet et al., 2010; Zhou et al., 2010) and the inhibitory PD1 receptor was recently shown to sustain the immune response in chronic infection. These cells have expansion capacity and continuously produce more differentiated $Tcf1^{-}$ $PD1^{+}$ CD8 T cells while maintaining a pool of $Tcf1^{+}$ cells (Utzschneider et al., 2016) (Wu et al., 2016). CD8 T cells with corresponding properties were identified based on Cxcr5 expression, which overlaps considerably with that of Tcf1 (Im et al., 2016). $Cxcr5^{+}$ CD8 T cells reside in secondary lymphoid tissues of chronically infected mice, predominantly in the T cell zone (Im et al., 2016). Here we addressed whether similar to the immune response in chronic viral infection, spontaneous or immunotherapy driven anti-tumor CD8 T cell responses involved a memory component and, if so, whether this component was part of the tumor microenvironment. We found that tumor-specific $Tcf1^{+}$ $PD1^{+}$ CD8 T cells resided in the tumor microenvironment and that they were critical for immune control of cancer promoted by immunotherapy.

RESULTS

Lack of Tcf1 in tumor-reactive CD8 T cells diminishes tumor control in response to therapeutic vaccination

To address whether CD8 T cell responses to tumors or the beneficial effects of immunotherapy involved a memory component we tested whether such responses depended on the central memory transcription factor Tcf1 (Jeannet et al., 2010; Zhou et al., 2010). CD8 T cells specific for the surrogate tumor antigen LCMV gp33 (P14) (CD45.2) were adoptively transferred into naive C57BL/6 (B6) mice (CD45.1). One day later such P14 chimeric mice were implanted subcutaneously (s.c.) with B16 melanoma cells expressing LCMV gp33 (B16-gp33) (**Fig. 1A**). This approach was used to follow tumor-specific CD8 T cells and to determine whether these cells or subsets thereof were relevant for tumor control.

The time until tumors reached a size of $1cm^3$ (endpoint) was modestly and comparably extended in wild type (WT) and *Tcf7*$^{-/-}$ P14 chimeric mice (not shown). Mice were thus vaccinated using gp33 peptide plus adjuvant (TLR3 ligand (poly(I:C)) when tumors became palpable. The combination of vaccination and WT or *Tcf7*$^{-/-}$ P14 cell transfer resulted in transient tumor regression around one week post vaccination (**Fig. 1B, C**). The protective effect of *Tcf7*$^{-/-}$ P14 cells was short-lived as compared to WT P14 cells (**Fig. 1B, C)**. This correlated with a 10 fold higher abundance of WT as compared to *Tcf7*$^{-/-}$ P14 tumor-infiltrating lymphocytes (TIL) at endpoint (**Fig. 1D**). In contrast, when TIL were analyzed approximately one week after vaccination (intermediate time point), WT and *Tcf7*$^{-/-}$ P14 TIL were equally abundant (**Fig. 1E**). Thus, P14 TIL lacking *Tcf7* were abundant early post vaccination but declined thereafter and this correlated with reduced tumor control.

Tumor-specific TIL harbor prominent subsets of Tcf1$^+$ PD1$^+$ and Tcf1$^-$ PD1$^+$ CD8$^+$ T cells

Since extended tumor control depended on Tcf1, we characterized Tcf1 expression in WT P14 cells in both vaccinated as well as non-treated mice (**Fig. 1A**). Naive P14 cells were homogenously Tcf1$^+$ (see e.g. **Fig. 3A**). Similarly most P14 TIL in palpable tumors (<$100mm^3$) of untreated mice were Tcf1$^+$ but also expressed PD1 (**Fig. 2A**), indicating that they had been exposed to antigen. The abundance of Tcf1$^+$ PD1$^+$ P14 TIL was increased (8 fold) when tumors had an intermediate size (200-$300mm^3$), but declined in large tumors at endpoint ($1cm^3$) (**Fig. 2A, B)**. Therapeutic vaccination of mice with palpable tumors robustly expanded Tcf1$^+$ PD1$^+$ P14 TIL (176 fold) one week later and these cells remained present at elevated levels at endpoint (**Fig. 2A, C)**. P14 TIL also included a prominent Tcf1$^-$ PD1$^+$

subset, which expanded and contracted in parallel with Tcf1$^+$ PD1$^+$ TIL and appeared more differentiated based on the frequent co-expression of GzmB. Corresponding results were obtained when Tcf1 expression was followed using a *Tcf7*-GFP reporter (Utzschneider et al., 2016) (not shown). To assess whether the isolated CD8 T cells derived from the tumor we performed *in vivo* vascular cell labeling. Unlike blood borne P14 cells, which were homogenously stained with the i.v. injected fluorescent CD8α Ab, the vast majority (95%) of *Tcf7*-GFP$^+$ and *Tcf7*-GFP$^-$ P14 cells isolated from tumors were not labeled (**Fig. S1A),** which indicated that both subsets resided in the tumor. Thus Tcf1$^+$ PD1$^+$ TIL were constitutively present in the tumor, their abundance transiently increased as tumors progressed and these cells could be expanded further by therapeutic vaccination.

The Tcf1$^+$ PD1$^+$ P14 cells were also present in the tumor-draining lymph node (dLN) (**Fig S1B)** and spleen of vaccinated mice (not shown). While Tcf1$^+$ PD1$^+$ P14 cells were observed in the tumor of non-vaccinated mice, P14 cells present in the dLN (**Fig S1B)** or the spleen did not express PD1 (not shown), indicating that the latter were not persistently exposed to antigen. Notwithstanding peripheral P14 cells expressed CD44 (not shown) implying that they were antigen-experienced.

Vaccination thus amplified tumor-specific CD8 TIL but was not critical to establish the observed TIL subset distribution (**Fig. 2A, B)**. This conclusion was supported by the presence of the corresponding TIL subsets amongst host CD8 T cells (**Fig. 2A).** Analogous results were obtained using a different melanoma cell line (YUMM-OVA) recognized by distinct tumor-specific CD8 T cells (OT-1) (**Fig. S1C**), using a thymoma cell line (E.G7-gp33) (**not shown**) and during adoptive T cell therapy experiments (**Fig. S1D**). We further addressed the presence of Tcf1$^+$ PD1$^+$ cells amongst polyclonal CD8 TIL. B16-gp33 melanoma cells were implanted into *Tcf7*-GFP reporter mice and CD8 TIL specific for gp33 or the tumor-associated gp100 or Trp2 antigens were identified using tetramer staining. While most tumor-specific polyclonal CD8 TIL were *Tcf7*-GFP$^-$ PD1$^+$, we also detected a population of *Tcf7*-GFP$^+$ PD1$^+$ TIL (**Fig. 2D, S1E** and not shown). A corresponding subset distribution was observed following vaccination (using a pool of peptides plus adjuvant) and when gp33 tetramer$^+$ TIL were analyzed for Tcf1 protein instead of *Tcf7*-GFP reporter expression (**Fig. S1F**). Vaccination significantly expanded both the *Tcf7*-GFP$^+$ and the *Tcf7*-GFP$^-$ TIL subsets (**Fig. 2D, E, S1E**). We concluded that Tcf1$^+$ PD1$^+$ CD8 TIL specific for distinct tumor antigens arise during spontaneous anti-tumor immune responses and that these cells can be expanded by therapeutic vaccination.

Since Tcf1$^+$ PD1$^+$ CD8$^+$ T cells were extravascular (**Fig. S1A**) we next used immunofluorescence staining to localize these cells in B16-gp33 tumors of vaccinated mice. P14 cells (CD45.2$^+$) were

scattered throughout the tumor. Tcf1$^+$ P14 cells, detected either using the *Tcf7*-GFP reporter (**Fig. 2F**) or Tcf1 protein (**Fig. S1G**) appeared enriched in perivascular areas (CD31$^+$). Quantitative analyses confirmed the preferential localization of *Tcf7*-GFP$^+$ cells in the vicinity of endothelial structures (CD31$^+$) while *Tcf7*-GFP$^-$ cells localized deeper within the tumor parenchyma (**Fig. 2G**). Corresponding localizations were observed in non-vaccinated mice (**Fig. S1H**). In vaccinated mice, *Tcf7*-GFP$^+$ cells were part of T cell rich, but B cell poor, perivascular infiltrates of hematopoietic cells. These infiltrates did not contain segregated T cell and B cell zones (**Fig. S1I)** and thus lacked the hallmarks of tertiary lymphoid structures (TLS). *Tcf7*-GFP$^+$ cells remained in relative proximity to tumor cells, as judged by their localization close to GFP expressing B16-gp33 cells (**Fig. S1J**). Thus, Tcf1$^+$ CD8$^+$ T cells are present in the tumor microenvironment where they might contribute to a local immune response even in the absence of bona fide TLS.

Ablation of tumor-specific Tcf1$^+$ CD8 T cells curtails tumor control

To assess the importance of tumor-specific Tcf1$^+$ CD8 T cells in the tumor immune response and tumor control we generated a mouse strain, which allowed the selective ablation of Tcf1-expressing cells *in vivo*. We inserted a diphtheria toxin receptor (DTR) T2A green fluorescent protein (GFP) fusion gene into the *Tcf7* locus (**Fig. S2A**) and verified the proper expression and regulation of this *Tcf7*-DTR-GFP construct. In splenocytes from naive *Tcf7*-DTR-GFP P14 mice, GFP fluorescence was detected in essentially all P14 cells but not in B cells, in agreement with Tcf1 protein expression (**Fig. 3A**). Next, we generated *Tcf7*-DTR-GFP P14 chimeric mice and implanted them with B16-gp33 tumor cells. Mice were vaccinated when tumors became palpable and TIL were analyzed 6 days later (**Fig. 3B**). At this stage only a minority of P14 cells expressed GFP. Flow sorted *Tcf7*-DTR-GFP$^+$ P14 TIL expressed uniformly high levels of intracellular Tcf1 protein. Conversely, most *Tcf7*-DTR-GFP$^-$ P14 TIL lacked Tcf1 although a small subpopulation retained intermediate Tcf1 levels (**Fig 3C**). Identical results were obtained in splenic *Tcf7*-DTR-GFP P14 cells (**Fig S2B**) and using original *Tcf7*-GFP reporter (**Fig S2C**). These experiments ensured that GFP expression identified CD8 TIL retaining high levels of Tcf1 protein. Short term Diphtheria Toxin (DT) treatment efficiently deleted GFP$^+$ P14 TIL but had no effect on the abundance of GFP$^-$ P14 TIL (**Fig. S2D**), demonstrating that DT treatment was effective and had no direct effect on Tcf1$^-$ P14 TIL.

Tumor bearing mice were thus treated with DT, revaccinated to boost the immune response and analyzed 16 days later (**Fig. 3B)**. DT exposure resulted in a near complete absence of P14 cells

expressing GFP (**Fig. S2F**) or Tcf1 protein from TIL (**Fig. 3D**), the dLN (**Fig. S2E**) or the spleen (not shown) of *Tcf7*-DTR-GFP P14 chimeric mice. Elimination of Tcf1$^+$ P14 cells reduced the abundance of Tcf1$^-$ P14 cells present amongst TIL (2.5-fold) (**Fig. 3E, F**), the dLN (**Fig. S2E**) or the spleen (5-6 fold) (not shown). This was not due to DT toxicity since P14 cells were abundant in DT-treated *Tcf7*-GFP P14 chimeric mice (**Fig. 3E, F, S2E, F**). Thus, Tcf1$^+$ cells sustained the production of Tcf1$^-$ TIL.

The tumor volume (**Fig. 3G)** and tumor weight upon sacrifice (**Fig. 3H**) was low in *Tcf7*-DTR-GFP P14 chimeric mice. In contrast tumors progressed when Tcf1$^+$ P14 cells had been ablated. This was not due to DT toxicity, as tumors were controlled in DT-treated *Tcf7*-GFP P14 chimeric control mice (**Fig. 3G, H**). As P14 cells expressed PD1 prior to DT treatment (**Fig. 3C, S2B, C**), the data suggested that tumor-specific Tcf1$^+$ PD1$^+$ CD8 T cells were essential for robust anti-tumor immunity in response to therapeutic vaccination.

Intratumoral Tcf1$^+$ PD1$^+$ CD8 T cells mediate extended tumor control in response to therapeutic vaccination

Therapeutic vaccination resulted in tumor control depending on the presence of tumor-specific Tcf1$^+$ PD1$^+$ CD8 T cells. We next determined the contribution of tumor-resident as opposed to peripheral Tcf1$^+$ CD8 T cells to the treatment response. We used the sphingosine 1-phosphate receptor-1 (S1PR1) inhibitor FTY720 to prevent the exit of T cells from lymphoid organs and thus to block the influx of new T cells into the tumor (Mandala et al., 2002) (**Fig. 4A**). Just prior to FTY720 and DT treatment all P14 TIL expressed PD1 and a subset of around 15% was *Tcf7*-DTR-GFP$^+$ (**Fig. 4B**).

At the time of sacrifice, the abundance of circulating CD3$^+$ T cells was reduced >90% in FTY720 treated animals (**Fig. 4C**), showing that T cell exit from lymphoid organs was blocked similar to published data (Spranger et al., 2014). As above, DT-treatment resulted in the complete absence of GFP$^+$ (not shown) or Tcf1$^+$ P14 TIL in *Tcf7*-DTR-GFP P14 chimeric mice **(Fig. 4D)**. Preventing the influx of new lymphocytes did not impact the abundance of P14 TIL (**Fig. 4F**). However, when lymphocyte immigration was blocked and Tcf1$^+$ P14 TIL were depleted (initially around 15% of P14 TIL (**Fig. 4B**)) the abundance of Tcf1$^-$ P14 TIL was reduced 6-7 fold (**Fig. 4F**). Thus in the absence of Tcf1$^+$ PD1$^+$ TIL the differentiated Tcf1$^-$ PD1$^+$ GzmB$^+$ compartment was greatly compromised, implying that intratumoral Tcf1$^+$ PD1$^+$ TIL were the source of these cells. At the same time a population of Tcf1$^+$ PD1$^+$ TIL was maintained, indicating that these cells self-renewed within the tumor microenvironment. Tumors were controlled even when the influx of new T cells was prevented (**Fig. 4G-H**). However,

when Tcf1$^+$ P14 TIL were ablated, tumors progressed. None of the above phenotypes were observed in DT-treated control *Tcf7*-GFP P14 chimeric mice (**Fig. 4D-H**). Thus tumor-resident Tcf1$^+$ PD1$^+$ cells mediated tumor control in response to therapeutic vaccination.

Tumor-control in response to checkpoint blockade immunotherapy depends on intrtumoral Tcf1$^+$ PD1$^+$ CD8 T cells

Co-inhibitory receptors such as PD1 and CTLA4 (Cytotoxic T Lymphocyte Antigen 4) restrain T cell antitumor immunity and their blockade mediates T cell-dependent tumor regression in preclinical animal models and cancer patients (Page et al., 2014). However, the cellular basis for the efficacy of this therapeutic intervention has remained unclear. Our own experiments showed that such checkpoint blockade immunotherapy (CBI) expanded P14 TIL in a Tcf1-dependent fashion and that the combination of CBI with the adoptive transfer of Tcf1-sufficient P14 cells mediated efficient tumor control (**Fig. S3**). These findings raised the possibility that Tcf1$^+$ CD8 T cells played a role for tumor control in response to CBI. Since intratumoral cells controlled tumors in response to vaccination (see above) or CBI (Spranger et al., 2014), we directly addressed whether intratumoral Tcf1$^+$ cells were required for tumor control in response to CBI (**Fig. 5A**).

We enrolled *Tcf7*-DTR-GFP P14 chimeric mice in CBI trials when B16-gp33 tumors were around 100mm^3. At this stage, all P14 TIL expressed PD1 and around 15% were *Tcf7*-DTR-GFP$^+$ (**Fig. 5B**). Influx of new T cells into the tumor was prevented using FTY720, Tcf1$^+$ P14 TIL were ablated using DT and CBI was initiated as schematically shown in (**Fig. 5A**).

Upon sacrifice, we confirmed FTY720-mediated depletion of CD3$^+$ cells from blood (>90%) and efficient DT-mediated deletion of *Tcf7*-DTR-GFP$^+$ P14 cells from TIL **(Fig. 5C**). As compared to isotype control treated mice, CBI increased the abundance of both Tcf1$^+$ and Tcf1$^-$ P14 TIL >10 fold. Elimination of Tcf1$^+$ TIL drastically reduced the abundance of Tcf1$^-$ P14 TIL (**Fig. 5D, E**). Thus CBI expanded intratumoral Tcf1$^+$ TIL and the presence of these cells was essential for the generation of differentiated Tcf1$^-$ TIL. Even though the influx of new T cells was blocked, tumors in CBI treated animals were controlled (**Fig. 5F-G**)**.** However, tumor control was lost when Tcf1$^+$ P14 TIL were ablated. None of these effects were observed in DT-treated control *Tcf7*-GFP P14 chimeric mice (**Fig. 5F-G**). Thus tumor-specific Tcf1$^+$ CD8 T cells that expressed PD1 and that resided in the tumor microenvironment mediated tumor control in response to CBI.

Intratumoral Tcf1$^+$ PD1$^+$ CD8 T cells have stem-like properties while displaying features of exhausted cells

Given the importance of Tcf1$^+$ PD1$^+$ TIL for tumor control we molecularly characterized these cells in comparison to established CD8 T cell populations. Intratumoral P14 cells were flow sorted on d7 post vaccination and subjected to RNAseq analysis. Principal component analysis (PCA) identified *Tcf7*-GFP$^+$ and *Tcf7*-GFP$^-$ TIL as discrete populations of cells distinct from naive splenic *Tcf7*-GFP$^+$ cells (Naive) (**Fig. 6A**). In agreement with these data 569 genes were differentially expressed between *Tcf7*-GFP$^+$ and *Tcf7*-GFP$^-$ TIL (False Discovery Rate (FDR) <5% and fold-change (FC) >2) (**Table S1). "**Cytokine-cytokine receptor interaction" represented the KEGG pathway term most significantly associated with upregulated (p=1.45e-8) and with downregulated genes (p=3.8e-8). TIL subsets were next compared to CD8 T cells from chronic and acute resolved LCMV infections (Utzschneider et al., 2016). The PC1 versus PC2 separated tumor and infection derived CD8 T cell population (**Fig. S4A**), indicating considerable differences between these cells. Notwithstanding, PC2 versus PC3 showed that *Tcf7*-GFP$^-$ TIL clustered with exhausted cells (*Tcf7*-GFP$^-$ cells from chronic LCMV infection). On the other hand the *Tcf7*-GFP$^+$ populations were more diverse. *Tcf7*-GFP$^+$ TIL clustered more closely to memory-like cells (*Tcf7*-GFP$^+$ cells from chronic LCMV infection) than to central memory cells (*Tcf7*-GFP$^+$ cells from acute resolved LCMV infection) (**Fig. 6B).** In agreement with these data, *Tcf7*-GFP$^+$ TIL and memory-like cells expressed unique genes but also a considerable number of shared genes (n=443, FDR <5%, FC >2) (**Fig. S4B, Table S2),** including Ly108 (Slamf6) or Cxcr5 (**Fig. 6D, S4C**). Thus, despite their distinct biological context and tissue origin, the gene signatures of *Tcf7*-GFP$^+$ TIL and chronic infection-derived cells significantly overlapped (**Fig. 6C**). The KEGG pathway terms "Cytokine-cytokine receptor interaction" and "Natural killer cell mediated cytotoxicity" were most significantly associated with shared upregulated (p=3.3e-10) and downregulated genes (p=2.53e-5), respectively.

The transcriptome of *Tcf7*-GFP$^+$ TIL showed significant enrichment of a memory precursor (MPEC) gene set (Joshi et al., 2007) (**Fig. 6C**) and expressed several central memory markers (*Tcf7*, *Sell* (CD62L), *Ccr7*, *Id3, Bcl6*) at levels corresponding to or above those of central memory cells (**Fig. 6D, S4D**). Interestingly the transcriptome of *Tcf7*-GFP$^+$ TIL was distinct form skin-derived tissue resident memory (T_{RM}) cells (Mackay et al., 2013) (**Fig. 6C**) and (Mackay et al., 2016) (**Fig. S4E**). Indeed, *Tcf7*-GFP$^+$ TIL expressed low levels of several key genes associated with T_{RM} including *Prdm1* (Blimp1)*, Zfp613* (Hobit) and *Runx3* (**Fig. S4F**). Rather, the T_{RM} signature was significantly enriched in *Tcf7*-

GFP$^-$ TIL (**Fig. 6C, S4C**) and the expression of certain T_{RM} genes was increased in *Tcf7*-GFP$^-$ as compared to *Tcf7*-GFP$^+$ TIL (**Fig. S4F**). These data suggested that Tcf1$^+$ PD1$^+$ TIL lacked T_{RM} features, but that they produced intratumoral progeny with T_{RM} characteristics.

Functionally, *Tcf7*-GFP$^+$ TIL produced IL2 both spontaneously and following restimulation (**Fig. 6E**), a considerable fraction of these cells cycled based on KI67 expression and DNA content analysis (**Fig. S4G**) and these cells were less prone to undergo apoptosis as compared to *Tcf7*-GFP$^-$ TIL (**Fig. S4H**). To assess the expansion potential of these cells we transferred flow sorted P14 TIL (CD45.2) into naive secondary recipients (CD45.1) followed by LCMV infection. While transferred *Tcf7-GFP*$^-$ P14 TIL essentially failed to expand, *Tcf7-GFP*$^+$ P14 TIL expanded significantly **(Fig. 6F).** Progeny of *Tcf7-GFP*$^+$ P14 TIL were predominantly *Tcf7*-GFP$^-$ although a subpopulation of *Tcf7*-GFP$^+$ cells was also present and these cells had expanded as compared to input (**Fig. 6G**). Thus transferred *Tcf7*-GFP$^+$ TIL had the potential to expand, differentiate and reproduce *Tcf7*-GFP$^+$ cells, which was consistent with the conclusions based on the *in vivo* ablation of Tcf1$^+$ P14 TIL (**Fig. 4**). In agreement with these stem cell-like properties, transcripts upregulated in *Tcf7-GFP*$^+$ P14 TIL significantly overlapped with a subset of genes expressed by adult stem cells (Wong et al., 2008) or by hematopoietic stem/progenitor cells but not by mature hematopoietic cells (Ivanova et al., 2002) (**Fig. S5A**).

Conversely, the transcriptome of short lived effector cells (SLEC) (Joshi et al., 2007) was not enriched in *Tcf7*-GFP$^+$ TIL (**Fig. 6C)** and selected genes or proteins involved in effector T cell differentiation or function were expressed at low levels in *Tcf7*-GFP$^+$ TIL (**Fig. 6H, S5B, C**). Further, *Tcf7*-GFP$^+$ TIL produced less IFNγ but equal amounts of TNFα (not shown) as compared to *Tcf7*-GFP$^-$ TIL (**Fig. 6E**)**.** Finally, Tcf1$^+$ TIL expressed less T-bet but more Eomes as compared to Tcf1$^-$ TIL (**Fig. S5C**), similar to observations in chronic viral infection (Utzschneider et al., 2016) (Im et al., 2016).

Despite the relative lack of an effector program, *Tcf7*-GFP$^+$ TIL expressed multiple exhaustion markers (*Lag3, Pdcd1, CTLA4*) usually at slightly lower levels than *Tcf7*-GFP$^-$ TIL (**Fig. 6I, S5D, E**). Additional exhaustion-associated genes were more selectively expressed by *Tcf7*-GFP$^-$ TIL (*Maf*, *Cd244* (2B4) *Havcr2* (Tim3), *Ccl3*) (**Fig. S5D**), indicating that upregulation of these genes was associated differentiation.

Finally, the transcriptome of *Tcf7*-GFP$^+$ TIL was significantly enriched with the signature of follicular helper (T_{FH}) T cells (**Fig. 6C**) similar to memory-like cells (not shown) (Im et al., 2016). Thus, despite the fact that the cells persist in very different environments, Tcf1$^+$ PD1$^+$ CD8 T cells present in tumors are remarkably similar to memory-like CD8 T cells in the spleens of mice with chronic viral infection.

To address the importance of Tcf1 in the generation or function of *Tcf7*-GFP$^+$ TIL, we analyzed *Tcf7*-GFP reporter mice that were knock out for *Tcf7* (KO *Tcf7*-GFP). Naive P14 cells from KO *Tcf7*-GFP mice expressed high levels of GFP (**Fig. S6A**) demonstrating that *Tcf7* expression did not depend on Tcf1 protein and that KO reporter cells were useful to determine the role of Tcf1 in these stem-like cells. KO or WT *Tcf7*-GFP P14 chimeric mice were implanted with B16-gp33 cells and mice were vaccinated when tumors became palpable (**Fig. S6B**). One week later, we observed a comparable abundance of WT and KO P14 TIL (**Fig. S6C**), consistent with (**Fig. 1E**). The abundance of *Tcf7*-GFP$^+$ TIL was also comparable (**Fig. S6C**), demonstrating that the generation of this TIL subset cells did not depend on Tcf1 protein. To address the function of KO *Tcf7*-GFP$^+$ TIL we prevented the influx of new T cells into the tumor and re-challenged the cells by vaccination. One week later, KO P14 TIL were drastically reduced as compared to WT. Moreover, this was associated with a drastic reduction of KO *Tcf7*-GFP$^+$ P14 TIL compared to WT (**Fig. S6D**). Thus, Tcf1 protein was essential to maintain the *Tcf7*-GFP$^+$ TIL population in response to restimulation.

To begin to address the gene expression program(s) controlled by Tcf1, we combined our RNAseq analyses with Tcf1 ChIPseq data from naïve CD8 T cells (Xing et al., 2016). Considering Tcf1 binding peaks within ±5kb of genomic sequence flanking a gene, naïve CD8 T cells had 5220 Tcf1-bound genes. Among 260 genes upregulated in *Tcf7-GFP*$^+$ TIL 71 (27.3%) were bound by Tcf1, while 73 of the 309 downregulated genes (23.6%) were bound by Tcf1 in naive CD8 T cells (**Table S1)**. While there was no specific KEGG term associated with these genes, we noted several effector genes among Tcf1-bound repressed genes (e.g. *Granzymes, Id2, KLRG1*). Thus Tcf1 may maintain *Tcf7*-GFP$^+$ TIL at least in part by counteracting cellular differentiation.

Presence of TCF1$^+$ PD1$^+$ CD8$^+$ T cells in melanoma patients

We next addressed whether tumor-reactive TCF1$^+$ PD1$^+$ CD8 T cells were present in human cancer patients. To this end stained peripheral blood CD8 T cells of Melan A peptide vaccinated melanoma patients with Melan A tetramer (MelA). As naive T cells express TCF1, we restricted all our analyses to non-naive CD95$^+$ CD58$^+$ MelA$^+$ CD8 T cells. Such cells contained a major subpopulation of Tcf1^{low} CCR7^{low} cells (90-99%) and a minor population of Tcf1^{hi} CCR7^{hi} cells (0.2-10%) (**Fig. 7A, S7A**). The latter included sizeable fractions of PD1$^+$ cells in 4 of the 5 patients (**Fig. 7B, S7A**). This was specific to tumor-reactive cells since non-naive Tcf1^{hi} CCR7^{hi} cells present among total CD8 T cells did not express PD1 (**Fig. 7B**). In addition to the markers used for gating, MelA Tcf1^{hi} CCR7^{hi} PD1$^+$ CD8 T

cells expressed IL7Rα, CD45RA, CD69 and CXCR5 on a small fraction of cells (**Fig. S7B)**. MelA^{+} TCF1^{low} CCR7^{low} cells also included a considerable fraction of PD1^{+} cells (30-50%) (**Fig. 7B**). These cells essentially lacked IL7Rα and were bimodal for CD45RA (**Fig. S7B**). Thus similar to anti-tumor immune responses in mice, the blood of melanoma patients harbored tumor-specific TCF1^{+} PD1^{+} CD8 T cells as well as TCF1^{-} PD1^{+} cells with the same antigen specificity.

To identify corresponding T cells in melanoma tumors we used multiplex staining combined with digital image-based cell quantification. These analyses readily identified TCF1^{+} PD1^{+} CD8 T cells in human melanoma (**Fig. 7C-G**). Such cells preferentially localized to stromal regions and were essentially undetectable in the tumor bed (as distinguished in **Fig. 7C, E)**. TCF1^{-} PD1^{+} CD8 T cells were also detected in the tumor but were more frequent in the stroma (**Fig. S7C**). The abundance of stromal TCF1^{+} PD1^{+} cells correlated with that of TCF1^{-} PD1^{+} cells present in the stroma (p=0.090) or the tumor (p=0.050) (**Fig. S7C**), suggesting that the abundance of differentiated TCF1^{-} PD1^{+} TIL was related to the presence of TCF1^{+} PD1^{+} TIL. Structures resembling TLS were noted in 4 out of 13 patients and some of these TLS harbored TCF1^{+} PD1^{+} CD8 T cells both in the T cell zone and the putative B cell zone (**Fig. S7D-F**). Clearly, however, TCF1^{+} PD1^{+} CD8 T cells were observed in the absence of TLS, similar to murine tumors (**Fig. S1I**).

To further characterize TCF1^{+} PD1^{+} CD8 TIL we reanalyzed publically available single cell RNAseq data of human melanoma-infiltrating CD8 T cells (Tirosh et al., 2016). These analyses identified subpopulations of *CD8A*$^{+}$ TIL that co-expressed *TCF7 and PDCD1* (PD1) in two patients (**Fig. 7H, S7G)**. Many *TCF7*$^{+}$ *PDCD1*$^{+}$ *CD8A*$^{+}$ TIL expressed central memory associated genes (e.g. *TCF7, SELL, IL7Ra*), lacked effector genes (e.g. *PRDM1, GZMA*) but expressed exhaustion-associated genes (e.g. *PDCD1, LAG3, TIGIT*) **(Fig. 7I, S7H).** Abundant *TCF7*$^{-}$ *PDCD1*$^{+}$ *CD8A*$^{+}$ TIL were also detected. These cells generally lacked central memory genes, but expressed both effector and exhaustion associated genes **(Fig. 7I, S7H).** Thus human melanomas harbor *TCF7*$^{+}$ *PDCD1*$^{+}$ CD8 TIL with gene expression profiles similar to cells identified in the mouse models.

Since some of the single cell RNAseq data derive Ipilimumab (anti-CTLA4) and/or Nivolumab (anti-PD1) treated patients (Tirosh et al., 2016) we assessed the impact of checkpoint blockade on the CD8 TIL compartment. Patients treated with Ipilimumab and/or Nivolumab showed a higher fraction of *TCF7*$^{+}$ *PDCD1*$^{+}$ cells amongst *CD8A*$^{+}$ TIL than untreated or alternatively treated patients (**Fig. S7I**). Thus *TCF7*$^{+}$ *PDCD1*$^{+}$ CD8 cells responded preferentially to checkpoint blockade. Finally we interrogated the Cancer Genome Atlas (TCGA) for correlations with patient survival in the melanoma

cohort. The analysis of primary melanomas (i.e. excluding lymph node metastases) showed that CD8 T cell infiltration (average expression of *CD8A, CD8B, CD2, CD3G, CD3E* and *CD3D*) had a prognostic value in agreement with (Fridman et al., 2012)**.** We thus focused on melanomas with a high level of T cell infiltration. Among these patients, *TCF7* or *PDCD1* expression did not have prognostic value. However, the combined expression of *TCF7* and *PDCD1* had significant power to predict overall improved patient survival (**Fig. S7J**). Thus, meta-analysis of the TCGA database indicates that a *TCF7/PDCD1* signature correlates with improved patient survival.

DISCUSSION

Here we showed that intratumoral Tcf1$^+$ PD1$^+$ CD8 T cells mediated tumor control in response to immunotherapy. We referred to these cells as memory-like CD8 T cells as they persisted in the presence of antigen and displayed considerable phenotypic differences compared to conventional central memory cells. We identified similar cells among tumor antigen-reactive CD8 T cells in the blood of melanoma patients and among the CD8 T cell infiltrate of melanomas. The transcriptome of Tcf1$^+$ PD1$^+$ CD8 TIL resembled that of adult tissue-specific stem cells as well as hematopoietic stem /progenitor cells. Indeed, this TIL subpopulation displayed stem-like properties including the capacity to expand, self-renew and differentiate into Tcf1$^-$ PD1$^+$ TIL in the tumor microenvironment. It may be worth pointing out that the functional properties of memory-like CD8 T cells have so far been deduced from cell transfer experiments (Utzschneider et al., 2016) (Im et al., 2016). Such experiments address the developmental potential of these cells, but not necessarily their physiological role. Here we established an *in vivo* cell ablation approach and confirmed the stem-like properties of Tcf1$^-$ PD1$^+$ cells in the context of their tissue of residence and independent of a need of proper homing following adoptive transfer.

Tcf1$^+$ PD1$^+$ TIL showed striking molecular and functional similarities to memory-like cells present chronic viral infections (Utzschneider et al., 2016) (Im et al., 2016). This was remarkable given the very different biological contexts and tissue origins of these cells and it is tempting to speculate that corresponding cells may exist in additional situations of chronic antigen stimulation. Notwithstanding, we did also noted differences between the two types of CD8 T cells. Most strikingly, CXCR5$^+$ memory-like CD8 T cells in chronically infected mice are restricted to secondary lymphoid tissues (Im et al., 2016). In contrast, Tcf1$^+$ PD1$^+$ CD8 T cells persisted and functioned outside secondary lymphoid tissues, in tumor tissues. While these cells were detected in occasional TLS of human melanomas, they were clearly also present independent of TLS, both in human and in murine tumors. In the latter instance, specific perivascular niches may ensure the persistence of memory-like CD8 T cells in tumors.

Naive tumor-specific T cells are thought to expand and differentiate in the tumor draining lymph node and differentiated T cells home to the tumor (Chen and Mellman, 2017). Our date raise the possibility that tumors are also infiltrated by activated but relatively undifferentiated tumor-reactive Tcf1$^+$ CD8 T cells, where they can persist and sustain the tumor immune response. There is indeed growing evidence that the tumor microenvironment supports T cell-mediated tumor immune responses. For

example, intratumoral T cells proliferate during spontaneous tumor immune responses in mice (Horton et al., 2018) and in response to checkpoint blockade in melanoma patients (Tumeh et al., 2014). Mouse models suggest that the proliferative response to PD1-blockade depends on CD28-mediated co-stimulation (Kamphorst et al., 2017) and such data are in line with a role for intratumoral $CD103^+$ dendritic cells (DC) to re-stimulate and expand tumor-specific $CD8^+$ T cells (Broz et al., 2014). Finally, the local immune response has protective potential as transferred tumor-specific CD8 T cells (as shown herein) or endogenous TIL (Spranger et al., 2014) prevented tumor progression in response to checkpoint blockade even when the influx of new T cells was prevented.

Checkpoint blockade mediates a proliferative response of TIL, however, the cellular and molecular basis for this response has remained obscure since tumor-reactive CD8 T cells have an exhausted phenotype (Baitsch et al., 2011; Gros et al., 2014). Either, checkpoint blockade de-differentiated terminally differentiated T cells or it acted on less differentiated T cells that then produced an expanded pool of differentiated T cells. Our findings provide strong support for the latter scenario and suggest that expansion and differentiation can occur in the tumor. Indeed ablation of intratumoral $Tcf1^+$ $PD1^+$ cells revealed that $Tcf1^-$ $PD1^+$ $CD8^+$ TIL lacked expansion capacity and that the residual cells were not sufficient to maintain tumor control. In addition to TIL expansion, blockade of inhibitory receptors also improves T cell effector functions including cytokine production and cytotoxicity. We expect that the improved effector functions predominantly stem from the de-inhibition of differentiated $Tcf1^-$ $PD1^+$ TIL. If so, $Tcf1^-$ $PD1^+$ TIL may be more directly responsible for tumor control. However, they may only do so effectively when de-inhibited and when produced in sufficient numbers from $Tcf1^+$ precursors. The differentiation of TIL was associated with the loss of Tcf1 expression, raising the question regarding the relevant signals and the causal relationship. Using dendritic cell vaccinations, we have recently shown that inflammatory signals silence Tcf1 in activated T cells and that this facilitated effector differentiation (Danilo et al., 2018). Similarly, inflammatory cues may suppress Tcf1 in the tumor to facilitate differentiation. Indeed Tcf1-bound suppressed target genes include several effector genes.

While inhibitory receptor blockade has revolutionized cancer care, this intervention is still only effective in a minority of cancer patients. Thus there is a need to improve but also a considerable interest to predict, which patients will benefit. Clinical responses correlate with preexisting $CD8^+$ T cell infiltration and the neoantigen burden (Tumeh et al., 2014) (Schumacher and Schreiber, 2015). Our data suggest that clinical responses further depend on the presence of memory-like CD8 T cells. Our preliminary

analysis of a small cohort of pretreatment melanoma samples indicated that both responder and non-responder patients do have TCF1$^+$ PD1$^+$ TIL. While larger cohorts will be needed to determine whether the abundance of these cells differs between responders and non-responders, their presence in non-responders does not contradict the findings reported herein. The preclinical mouse models showed that Tcf1$^+$ PD1$^+$ cells are necessary for treatment response, but these cells are not likely sufficient. As discussed above, differentiated Tcf1$^-$ TIL are expected to play a role and the generation of the latter from Tcf1$^+$ precursors is likely controlled by additional signals. While this manuscript was under revision (Sade-Feldman et al., 2018) reported that the abundance of CD8 TIL expressing Tcf1 correlated with clinical response to checkpoint blockade. However, a majority of Tcf1$^+$ CD8 TIL usually lacks PD1 expression and may thus not recognize the tumor. It thus remains to be determined how these cells contribute to melanoma control in response to checkpoint blockade. Irrespectively, CD8 TIL displaying features of memory-like cells were reported in lung cancer patients based on low levels of PD1 (Thommen et al., 2018) or the expression of CXCR5 (Brummelman et al., 2018). Although the precise overlap between the distinct populations remains to be determined, memory-like CD8 T cells seem to be present in distinct human tumors.

Our investigations reveal a critical role of intratumoral CD8 T cells co-expressing Tcf1 and PD1 in immunotherapy-driven tumor control. The findings provide a basis for understanding how immune interventions impact immune responses against tumors. For example the data suggest that checkpoint blockade or vaccination does not rejuvenate differentiated cells but rather acts on less-differentiated memory-like CD8 T cells that produce an expanded pool of effector-type CD8 T cells. The identification of these stem-like cells will likely help to further improve all types of cancer immunotherapy.

ACKNOWLEDGMENTS

We are grateful to C. Fumey and M. Charmoy for mouse and lab management, H. Maby-El Hajjami for compiling the clinical data, the UNIL Flow Cytometry Facility (A. Wilson) for assistance, the UNIL Genomic Technology Facility (K. Harshman) for RNA sequencing and the Immune landscape laboratory, Center of experimental therapeutics, CHUV, (S. Rusakiewicz) for technical support.

SJC was supported by a SystemsX grant, DG is supported by the Swiss National Science Foundation (SNSF) (31003A_173156). SAL is supported in part by a grant from the SNSF (31003A-166161). DES is supported in part by grants the Swiss Cancer League (SCL) (KFS-3971-08-2016) and the SNSF (320030-152856, 310030-179459 and CRSII3-160708). WH is supported in part by grants from the SCL (KFS-3601-02-2015 and KFS-4407-02-2018) and the SNSF (310030_159598 and 310030B_179570).

AUTHOR CONTRIBUTIONS

I.S. designed and performed the majority of the experiments, K.S. performed the human histology, V.K. and D.P. performed experiments, S.F.M. performed the human PBL analysis, L.S. performed the murine histology, S.C.C .and S.P. analyzed the RNAseq data, S.J.C. and D.G. analyzed the ss RNAseq data. S.A.L. supervised the murine histology and provided critical input. D.E.S. supervised the human analyses and provided critical input and W.H. conceived the study, supervised the project and wrote the manuscript.

DECLARATION OF INTEREST

The authors declare no competing finacial interest.

REFERENCES

Baitsch, L., Baumgaertner, P., Devevre, E., Raghav, S.K., Legat, A., Barba, L., Wieckowski, S., Bouzourene, H., Deplancke, B., Romero, P.*, et al.* (2011). Exhaustion of tumor-specific CD8(+) T cells in metastases from melanoma patients. The Journal of clinical investigation *121*, 2350-2360.

Broz, M.L., Binnewies, M., Boldajipour, B., Nelson, A.E., Pollack, J.L., Erle, D.J., Barczak, A., Rosenblum, M.D., Daud, A., Barber, D.L.*, et al.* (2014). Dissecting the tumor myeloid compartment reveals rare activating antigen-presenting cells critical for T cell immunity. Cancer cell *26*, 638-652.

Brummelman, J., Mazza, E.M.C., Alvisi, G., Colombo, F.S., Grilli, A., Mikulak, J., Mavilio, D., Alloisio, M., Ferrari, F., Lopci, E.*, et al.* (2018). High-dimensional single cell analysis identifies stem-like cytotoxic CD8(+) T cells infiltrating human tumors. J Exp Med *215*, 2520-2535.

Chen, D.S., and Mellman, I. (2017). Elements of cancer immunity and the cancer-immune set point. Nature *541*, 321-330.

Danilo, M., Chennupati, V., Gomes Silva, J., Siegert, S., and Held, W. (2018). Suppression of Tcf1 by inflammatory cytokines facilitates effector CD8 T cell differentiation Cell Rep *22*, 2107-2117.

Fridman, W.H., Pages, F., Sautes-Fridman, C., and Galon, J. (2012). The immune contexture in human tumours: impact on clinical outcome. Nature reviews Cancer *12*, 298-306.

Gros, A., Robbins, P.F., Yao, X., Li, Y.F., Turcotte, S., Tran, E., Wunderlich, J.R., Mixon, A., Farid, S., Dudley, M.E.*, et al.* (2014). PD-1 identifies the patient-specific $CD8^{+}$ tumor-reactive repertoire infiltrating human tumors. The Journal of clinical investigation *124*, 2246-2259.

Gubin, M.M., Zhang, X., Schuster, H., Caron, E., Ward, J.P., Noguchi, T., Ivanova, Y., Hundal, J., Arthur, C.D., Krebber, W.-J.*, et al.* (2014). Checkpoint blockade cancer immunotherapy targets tumour-specific mutant antigens. Nature *515*, 577-581.

Horton, B.L., Williams, J.B., Cabanov, A., Spranger, S., and Gajewski, T.F. (2018). Intratumoral CD8+ T-cell Apoptosis Is a Major Component of T-cell Dysfunction and Impedes Antitumor Immunity. Cancer Immunol Res *6*, 14-24.

Im, S.J., Hashimoto, M., Gerner, M.Y., Lee, J., Kissick, H.T., Burger, M.C., Shan, Q., Hale, J.S., Lee, J., Nasti, T.H.*, et al.* (2016). Defining CD8+ T cells that provide the proliferative burst after PD-1 therapy. Nature *537*, 417-421.

Ivanova, N.B., Dimos, J.T., Schaniel, C., Hackney, J.A., Moore, K.A., and Lemischka, I.R. (2002). A stem cell molecular signature. Science (New York, N Y) *298*, 601-604.

Jeannet, G., Boudousquie, C., Gardiol, N., Kang, J., Huelsken, J., and Held, W. (2010). Essential role of the Wnt pathway effector Tcf-1 for the establishment of functional CD8 T cell memory. Proc Natl Acad Sci U S A *107*, 9777-9782.

Joshi, N.S., Cui, W., Chandele, A., Lee, H.K., Urso, D.R., Hagman, J., Gapin, L., and Kaech, S.M. (2007). Inflammation directs memory precursor and short-lived effector CD8(+) T cell fates via the graded expression of T-bet transcription factor. Immunity *27*, 281-295.

Kamphorst, A.O., Wieland, A., Nasti, T., Yang, S., Zhang, R., Barber, D.L., Konieczny, B.T., Daugherty, C.Z., Koenig, L., Yu, K.*, et al.* (2017). Rescue of exhausted CD8 T cells by PD-1-targeted therapies is CD28-dependent. Science (New York, N Y) *355*, 1423-1427.

Li, B., and Dewey, C.N. (2011). RSEM: accurate transcript quantification from RNA-Seq data with or without a reference genome. BMC Bioinformatics *12*, 323.

Mackay, L.K., Minnich, M., Kragten, N.A.M., Liao, Y., Nota, B., Seillet, C., Zaid, A., Man, K., Preston, S., Freestone, D.*, et al.* (2016). Hobit and Blimp1 instruct a universal transcriptional program of tissue residency in lymphocytes. Science (New York, N Y) *352*, 459-463.

Mackay, L.K., Rahimpour, A., Ma, J.Z., Collins, N., Stock, A.T., Hafon, M.-L., Vega-Ramos, J., Lauzurica, P., Mueller, S.N., Stefanovic, T.*, et al.* (2013). The developmental pathway for CD103(+)CD8+ tissue-resident memory T cells of skin. Nature immunology *14*, 1294-1301.

Mandala, S., Hajdu, R., Bergstrom, J., Quackenbush, E., Xie, J., Milligan, J., Thornton, R., Shei, G.-J., Card, D., Keohane, C.*, et al.* (2002). Alteration of lymphocyte trafficking by sphingosine-1-phosphate receptor agonists. Science (New York, N Y) *296*, 346-349.

Page, D.B., Postow, M.A., Callahan, M.K., Allison, J.P., and Wolchok, J.D. (2014). Immune modulation in cancer with antibodies. Annu Rev Med *65*, 185-202.

Prevost-Blondel, A., Zimmermann, C., Stemmer, C., Kulmburg, P., Rosenthal, F.M., and Pircher, H. (1998). Tumor-infiltrating lymphocytes exhibiting high ex vivo cytolytic activity fail to prevent murine melanoma tumor growth in vivo. Journal of immunology (Baltimore, Md : 1950) *161*, 2187-2194.

Reiser, J., and Banerjee, A. (2016). Effector, Memory, and Dysfunctional CD8(+) T Cell Fates in the Antitumor Immune Response. Journal of immunology research *2016*, 8941260.

Ribas, A., and Wolchok, J.D. (2018). Cancer immunotherapy using checkpoint blockade. Science (New York, N Y) *359*, 1350-1355.

Rosenberg, S.A., and Restifo, N.P. (2015). Adoptive cell transfer as personalized immunotherapy for human cancer. Science (New York, N Y) *348*, 62-68.

Sade-Feldman, M., Yizhak, K., Bjorgaard, S.L., Ray, J.P., de Boer, C.G., Jenkins, R.W., Lieb, D.J., Chen, J.H., Frederick, D.T., Barzily-Rokni, M.*, et al.* (2018). Defining T Cell States Associated with Response to Checkpoint Immunotherapy in Melanoma. Cell *175*, 998-1013 e1020.

Schaeuble, K., Britschgi, M.R., Scarpellino, L., Favre, S., Xu, Y., Koroleva, E., Lissandrin, T.K.A., Link, A., Matloubian, M., Ware, C.F.*, et al.* (2017). Perivascular Fibroblasts of the Developing Spleen Act as LTalpha1beta2-Dependent Precursors of Both T and B Zone Organizer Cells. Cell Rep *21*, 2500-2514.

Schumacher, T.N., and Schreiber, R.D. (2015). Neoantigens in cancer immunotherapy. Science (New York, N Y) *348*, 69-74.

Simoni, Y., Becht, E., and Fehlings, M. (2018). Bystander CD8+ T cells are abundant and phenotypically distinct in human tumor infiltrates. Nature.

Singer, M., Wang, C., Cong, L., Marjanovic, N.D., Kowalczyk, M.S., Zhang, H., Nyman, J., Sakuishi, K., Kurtulus, S., Gennert, D.*, et al.* (2016). A Distinct Gene Module for Dysfunction Uncoupled from Activation in Tumor-Infiltrating T Cells. Cell *166*, 1500-1511.e1509.

Speiser, D.E., Utzschneider, D.T., Oberle, S.G., Munz, C., Romero, P., and Zehn, D. (2014). T cell differentiation in chronic infection and cancer: functional adaptation or exhaustion? Nature reviews Immunology *14*, 768-774.

Spranger, S., and Gajewski, T.F. (2018). Impact of oncogenic pathways on evasion of antitumour immune responses. Nature reviews Cancer *18*, 139-147.

Spranger, S., Koblish, H.K., Horton, B., Scherle, P.A., Newton, R., and Gajewski, T.F. (2014). Mechanism of tumor rejection with doublets of CTLA-4, PD-1/PD-L1, or IDO blockade involves restored IL-2 production and proliferation of CD8(+) T cells directly within the tumor microenvironment. J Immunother Cancer *2*, 3.

Thommen, D.S., Koelzer, V.H., Herzig, P., Roller, A., Trefny, M., Dimeloe, S., Kiialainen, A., Hanhart, J., Schill, C., Hess, C.*, et al.* (2018). A transcriptionally and functionally distinct PD-1(+) CD8(+) T cell pool with predictive potential in non-small-cell lung cancer treated with PD-1 blockade. Nat Med *24*, 994-1004.

Tirosh, I., Izar, B., Prakadan, S.M., Wadsworth, M.H., 2nd, Treacy, D., Trombetta, J.J., Rotem, A., Rodman, C., Lian, C., Murphy, G.*, et al.* (2016). Dissecting the multicellular ecosystem of metastatic melanoma by single-cell RNA-seq. Science *352*, 189-196.

Tumeh, P.C., Harview, C.L., Yearley, J.H., Shintaku, I.P., Taylor, E.J., Robert, L., Chmielowski, B., Spasic, M., Henry, G., Ciobanu, V.*, et al.* (2014). PD-1 blockade induces responses by inhibiting adaptive immune resistance. Nature *515*, 568-571.

Utzschneider, D.T., Charmoy, M., Chennupati, V., Pousse, L., Ferreira, D.P., Calderon-Copete, S., Danilo, M., Alfei, F., Hofmann, M., Wieland, D.*, et al.* (2016). T Cell Factor 1-Expressing Memory-like CD8(+) T Cells Sustain the Immune Response to Chronic Viral Infections. Immunity *45*, 415-427.

Wei, S.C., Levine, J.H., Cogdill, A.P., Zhao, Y., Anang, N.-A.A.S., Andrews, M.C., Sharma, P., Wang, J., Wargo, J.A., Pe'er, D., and Allison, J.P. (2017). Distinct Cellular Mechanisms Underlie Anti-CTLA-4 and Anti-PD-1 Checkpoint Blockade. Cell *170*, 1120-1133.e1117.

Wherry, E.J., and Kurachi, M. (2015). Molecular and cellular insights into T cell exhaustion. Nature reviews Immunology *15*, 486-499.

Wong, D.J., Liu, H., Ridky, T.W., Cassarino, D., Segal, E., and Chang, H.Y. (2008). Module map of stem cell genes guides creation of epithelial cancer stem cells. Cell stem cell *2*, 333-344.

Wu, T., Ji, Y., Moseman, E.A., Xu, H.C., Manglani, M., Kirby, M., Anderson, S.M., Handon, R., Kenyon, E., Elkahloun, A.*, et al.* (2016). The TCF1-Bcl6 axis counteracts type I interferon to repress exhaustion and maintain T cell stemness. Sci Immunol *1*.

Wu, T., Shin, H.M., Moseman, E.A., Ji, Y., Huang, B., Harly, C., Sen, J.M., Berg, L.J., Gattinoni, L., McGavern, D.B., and Schwartzberg, P.L. (2015). TCF1 Is Required for the T Follicular Helper Cell Response to Viral Infection. Cell Rep *12*, 2099-2110.

Xing, S., Li, F., Zeng, Z., Zhao, Y., Yu, S., Shan, Q., Li, Y., Phillips, F.C., Maina, P.K., Qi, H.H.*, et al.* (2016). Tcf1 and Lef1 transcription factors establish CD8 T cell identity through intrinsic HDAC activity. Nature immunology *17*, 695-703.

Zhou, X., Yu, S., Zhao, D.M., Harty, J.T., Badovinac, V.P., and Xue, H.H. (2010). Differentiation and persistence of memory CD8(+) T cells depend on T cell factor 1. Immunity *33*, 229-240.

MAIN FIGURE TITELS AND FIGURE LEGENDS

Figure 1: Lack of Tcf1 in tumor-specific CD8 T cells reduces tumor control in response to therapeutic vaccination. (**A)** Experimental set up: B6 mice (CD45.1) were grafted with naïve wild type (WT) or *Tcf7*$^{-/-}$ P14 T cells (CD45.2) (WT or *Tcf7*$^{-/-}$ P14 chimeric mice). One day later mice were implanted s.c. with B16-gp33 tumor cells. When tumors became palpable, mice were vaccinated (gp33 peptide plus polyI:C) and analyzed 6 days later (intermediate) or when tumors were >1cm^3 (endpoint). (**B**) Tumor volume in WT P14 (open circle) or *Tcf7*$^{-/-}$ P14 chimeric mice (filled circle) or in the absence of P14 cells (No, black squares). (**C**) Fraction of mice with a tumor volume <1cm^3.

(**D, E**) Abundance of P14 cells (CD45.2$^+$) amongst gated CD8 tumor infiltrating lymphocytes (TIL) (per gram of tumor) in vaccinated mice (**D**) at endpoint and (**E**) 6 days post vaccination (intermediate).

Data in (**B**) are representative of 2 experiments with n=5 mice per group. Data in (**C-E**) are compiled from 2 experiments with n=8-10 mice per group. Error bars are SEM in (**B**) and SD in (**D, E**). Statistics is based on log rank test (**C**) or one-way Anova test (**D, E**).

Figure 2: Tumor-specific CD8 T cells include Tcf1$^+$ PD1$^+$ GzmB$^-$ and Tcf1$^-$ PD1$^+$ GzmB$^+$ subsets. (**A-C**) P14 TIL were analyzed when B16-gp33 tumors became palpable, at an intermediate (Interm.) time point or at endpoint (>1cm^3). Some mice were vaccinated when tumors became palpable and P14 TIL were analyzed 6 days later (Interm.) or at endpoint (>1cm^3). (**A**) Presence of P14 TIL (CD45.2$^+$) among gated CD8 TIL (top), Tcf1 versus Granzyme B (GzmB) expression in gated P14 TIL (middle) or in host CD8 TIL (bottom). Histogram overlays depict PD1 expression in Tcf1$^+$ (green) and Tcf1$^-$ P14 TIL (blue) as compared to host CD8 TIL (grey fill). (**B, C)** Abundance of Tcf1$^+$ (green) and Tcf1$^-$ P14 TIL (blue) per gram of tumor at the indicated stages of tumor progression (**B**) in non-vaccinated (Non-Vac.) mice (open circles) or (**C**) in vaccinated mice (filled circles). Data are compiled from 2 experiments with n=8 mice (palpable tumors) or are representative of at least 2 experiments with n=3-5 mice per group.

(**D, E**) Phenotypic analysis of polyclonal CD8 TIL. B16-gp33 tumor bearing *Tcf7*-GFP reporter mice were vaccinated (or not) with a mixture of gp33, gp100 and Trp2 peptides plus polyI:C and TIL were analyzed one week later. Gated CD44$^+$ gp33 tetramer$^+$ (gp33) CD8 TIL were analyzed for *Tcf7*-GFP and PD1 expression. (**E**) Abundance of *Tcf7*-GFP$^+$ gp33$^+$ TIL (green) and *Tcf7*-GFP$^-$ gp33$^+$ TIL (blue) per gram of tumor in untreated (open circles) and vaccinated mice (filled circles). Data are representative of 2 experiments each with n=3-5 mice per group.

(**F, G**) Localization of *Tcf7*-GFP P14 cells in B16-gp33 tumors 6 days post vaccination (**F**) Tissue sections were analyzed for P14 cells (CD45.2) (blue), *Tcf7*-GFP expression (green) and endothelial cells (CD31) (red). (**G**) Quantification of the mean distance (±SD) (in lymphocyte diameters) between $CD31^+$ cells and *Tcf7*-GFP^+ $CD45.2^+$ TIL (n=159) or Tcf7-GFP^- $CD45.2^+$ TIL (n=1084). Data are representative of 2 experiments. Statistics is based on unpaired t-test. See also Figure S1.

Figure 3: Extended tumor control in response to therapeutic vaccination depends on tumor-specific $Tcf1^+$ CD8 T cells.

(**A**) Expression of a *Tcf7*-diphtheria toxin receptor (DTR)-GFP fusion gene (green) (left) or Tcf1 protein (green) (right) in naïve P14 mice as compared to $CD19^+$ B cells (grey fill).

(**B**) Experimental approach.

(C) B16-gp33 TIL of *Tcf7*-DTR-GFP or *Tcf7*-GFP P14 chimeric mice were analyzed 6 days post vaccination. Gated *Tcf7*-DTR-GFP P14 TIL were analyzed for GFP expression (left). Tcf1 protein expression in flow sorted *Tcf7*-DTR-GFP^+ (green) and *Tcf7*-DTR-GFP^- P14 TIL (blue) as compared to $CD19^+$ B cells (grey fill) (middle) or PD1 expression in *Tcf7*-DTR-GFP^+ (green) and *Tcf7*-DTR-GFP^- P14 TIL (blue) as compared to host CD8 T cells (grey fill) (right).

(**D-H**) Analysis of P14 TIL following DT-mediated ablation of *Tcf7*-DTR-GFP^+ cells. Six days after vaccination mice were injected with diphtheria toxin (DT), revaccinated and analyzed 3 weeks later. (**D**) Gated P14 (CD45.2) (top) and host CD8 TIL (bottom) were analyzed for Tcf1 versus GzmB expression (**E**) Abundance of P14 TIL (CD45.2) amongst CD8 TIL. (**F**) Mean number (±SD) of P14 TIL per gram of tumor whereby $Tcf1^+$ (green) and $Tcf1^-$ P14 TIL (blue) are shown separately. (**G, H**) B16-gp33 tumor volume over time (**G**) or tumor weight at sacrifice (**H**).

Data in (**C**) are representative of 2 experiments. Data in (**D-G**) are representative of 2 experiments with n=5 mice per group. Error bars are SD in (**H**) and SEM in (**F, G**). Statistics is based on one-way Anova (**F, H**) or two-way Anova (**G**). Statistics in (**F**) is shown for total P14 TIL but is the same for $Tcf1^+$ (green) or $Tcf1^-$ P14 TIL (blue).

Figure 4: Extended tumor control in response to therapeutic vaccination depends on tumor-specific and tumor-resident $Tcf1^+$ $PD1^+$ CD8 T cells.

(**A**) B16-gp33 cell were implanted into *Tcf7*-DTR-GFP P14 chimeric mice, vaccinated when tumors became palpable and analyzed 6 days later. Mice were then treated with FTY720 (FTY) to prevent de

novo T cell immigration into the tumor, *Tcf7*-DTR-GFP$^+$ P14 cells were ablated using DT and mice were revaccinated.

(B) Validation 6 days post vaccination: GFP expression by gated *Tcf7*-DTR-GFP P14 (left) as compared to host CD8 TIL middle) and PD1 expression in *Tcf7*-DTR-GFP$^+$ (green) and *Tcf7*-DTR-GFP$^-$ P14 TIL (blue) as compared to host CD8 TIL (grey fill) (right).

(**C**) Efficacy of FTY720 treatment. Mean number (±SD) of CD3$^+$ T cells per ml of blood at d30 in non-treated control mice (black) as compared to FTY720-treated mice (open bars).

(**D-H**) Analysis of P14 TIL at d30. (**D**) Gated P14 (top) and host CD8 TIL (middle) were analyzed for the expression of Tcf1 versus GzmB or PD1 (bottom). (**E**) Gated CD8 TIL analyzed for the abundance of P14 TIL (CD45.2). (**F**) Mean numbers (±SD) of P14 TIL per gram of tumor whereby Tcf1$^+$ (green) and Tcf1$^-$ P14 TIL (blue) are shown separately.

(**G, H**) B16-gp33 tumor volume over time (**G**) or tumor weight at sacrifice (**H**).

Data in (**B**) are representative of 2 experiments. Data in (**C-H**) are representative of 2 experiments with n=5 mice per group. Error bars are SD in (**C, H**) and SEM in (**F, G**). Statistics is based on one-way Anova (**F, H**) or two-way Anova (**G**) tests. Statistics in (**F**) is shown for total P14 cells but is the same for Tcf1$^+$ (green) and Tcf1$^-$ P14 TIL (blue). See also Figure S2.

Figure 5: Extended tumor control in response to checkpoint blockade depends on intratumoral Tcf1$^+$ CD8 T cells.

(**A**) *Tcf7*-DTR-GFP P14 chimeric harboring B16-gp33 tumors of around 100mm^3 were exposed to FTY720 (FTY) (to prevent immigration of new lymphocytes into the tumor). *Tcf7*-GFP-DTR$^+$ P14 cells were ablated using DT and treatment with anti-PD1/CTLA4 Abs checkpoint blockade immunotherapy (CIB) or isotype control Ab was initiated.

(**B**) Validation prior to cell ablation. GFP expression by gated *Tcf7*-DTR-GFP P14 (left) as compared to host CD8 TIL middle) and PD1 expression in *Tcf7*-DTR-GFP$^+$ (green) and *Tcf7*-DTR-GFP$^-$ P14 TIL (blue) as compared to host CD8 TIL (grey fill).

(**C-E**) Analysis of P14 TIL at d26. (**C**) Gated P14 (top) and host CD8 TIL (bottom) were analyzed for the expression of Tcf1 versus GzmB. (**D**) and the abundance of P14 TIL (CD45.2) amongst gated CD8 TIL. (**E**) Mean number (±SD) of P14 TIL (per gram of tumor) whereby Tcf1$^+$ (green) and Tcf1$^-$ P14 TIL (blue) are shown separately.

(**F, G**) B16-gp33 tumor volume over time (**F**) or tumor weight at sacrifice (**G**).

Data in (**B**) are representative of 2 experiments. Data in (**C-G**) are representative of 2 experiments with n=5 mice per group. Error bars are SD in (**G**) and SEM in (**F, E**). Statistics is based on one-way (**E, G**) and two-way Anova (**F**). Statistics in (**E**) is shown for total P14 cells but is the same for Tcf1$^+$ (green) and Tcf1$^-$ P14 TIL (blue). See also Figure S3.

Figure 6: Tumor-specific Tcf1$^+$ PD1$^+$ CD8 TIL combine features of exhausted cells with stem-like properties.

Tcf7-GFP$^+$ and *Tcf7*-GFP$^-$ P14 TIL from B16-gp33 tumors were flow sorted 6 days post vaccination and subjected to RNA-seq analysis.

(A, B) Principal component analysis (PCA). (**A**) PCA of normalized gene reads in naive P14 cells (Naive) (open) versus *Tcf7*-GFP$^+$ TIL (green) and *Tcf7*-GFP$^-$ TIL (blue). (**B**) PCA of *Tcf7*-GFP$^+$ TIL (green) and *Tcf7*-GFP$^-$ TIL (blue) relative to P14 cells derived from chronic LCMV infection (*Tcf7*-GFP$^+$ LCMV cl13) (red) and *Tcf7*-GFP$^-$ LCMV cl13 (orange)) or *Tcf7*-GFP$^+$ P14 cells obtained after acute resolved LCMV infection (Central Memory) (black)). PC1 vs PC2 separated cells derived from tumors and viral infections (**Fig. S4A**). PC2 versus PC3 separated *Tcf7*-GFP$^+$ and *Tcf7*-GFP$^-$ cells. Each dot represents an individual mouse/sample.

(**C**) Gene set enrichment to identify similarities of the two TIL subsets with signatures of CD8 T cells responding to chronic LCMV infection (Utzschneider et al., 2016), or of memory precursors (MPEC) versus short lived effector cells (SLEC) (Joshi et al., 2007), or of tissue resident (T_{RM}) versus circulating memory CD8 T cells (T_{CIRC}) (Mackay et al., 2013) or of follicular CD4$^+$ helper cells (T_{FH}) versus helper 1 CD4 T cells (T_{H1}) (Wu et al., 2015). For each set, the number of genes (n), the direction of regulation (Dir, + =up-regulated and -=down-regulated) and the P value is indicated.

(**D-G**) Central memory features of P14 TIL subsets (**D**) Expression of selected markers of central memory or memory-like cells in *Tcf7*-GFP$^+$ (green) and *Tcf7*-GFP$^-$ P14 TIL (blue) as compared to host CD8 TIL (grey fill). (**E**) TIL were re-stimulated *in vitro* with gp33-peptide or not (no) or with PMA/Ionomycin (P/I). Gated *Tcf7*-GFP$^+$ (top) and Tcf7-GFP$^-$ P14 TIL (bottom) were analyzed for the expression of IL-2 and IFN-γ. The bar graphs shows the percentages of IL-2$^+$ (left) or of IFN-γ^+ (right) cells among *Tcf7*-GFP$^+$ (green) or *Tcf7*-GFP$^-$ P14 TIL (blue). (**F, G**) Proliferative, self-renewal and differentiation capacity of P14 TIL. (**F**) *Tcf7*-GFP$^+$ and *Tcf7*-GFP$^-$ P14 TIL (CD45.2) were flow sorted one week after vaccination and transferred into naive secondary Vβ5 recipients (CD45.1). Secondary recipients were infected with LCMV Arm, which causes acute resolved infection, and were analyzed 8

days later**.** Abundance of P14 cells (CD45.2$^+$) derived from *Tcf7*-GFP$^+$ or *Tcf7*-GFP$^-$ P14 TIL in the spleen of secondary recipients. (**G**) *Tcf7*-GFP expression in P14 cells present in the spleen of secondary recipients. Abundance of *Tcf7*-GFP$^+$ P14 cells (CD45.2$^+$) derived from *Tcf7*-GFP$^+$ P14 TIL in the spleen of secondary recipients as compared to input (assuming a take of 10%. (**H, I**) Analysis of effector and exhaustion features of P14 TIL subsets. Expression of selected proteins involved (**H**) in effector function/differentiation and (**I**) exhaustion in *Tcf7*-GFP$^+$/Tcf1$^+$ (green), *Tcf7*-GFP$^-$/ Tcf1$^-$ P14 TIL (blue) as compared to host CD8 TIL (grey fill).

Data in (**D, E, H, I**) are representative of at least 2 analyses with n=5 mice per group.

Data in (**F, G**) are from a single experiment using Vβ5 recipients, 2 additional experiments yielding comparable differences were performed using WT recipients, each experiment with n=5 mice per group. All error bars are SD. Statistics is based on two-tailed t test (**D, E**, **F, H, I**). For statistics in (**C**) see Experimental Procedures. See also Figure S4-6.

Figure 7: Identification and characterization of TCF1$^+$ PD1$^+$ CD8$^+$ T cells in melanoma patients.

(**A, B**) Analysis of peripheral blood lymphocytes (PBL) from melanoma patients. (**A**) Total CD8$^+$ T cells and MelanA-specific (MelA) CD8$^+$ T cells expressing CD58 and CD95 (non-naive), were analyzed for TCF1 and CCR7 expression (**B**) PD1 expression by gated non-naive MelA or non-naive CD8$^+$ T cells that are either Tcf1^{hi} CCR7^{hi} or Tcf1^{lo} CCR7^{lo} cells. Total effector memory (CCR7$^-$ CD45RA$^-$) (EM) and naive CD8 T cells (CCR7$^+$ CD45RA$^+$ CD95$^-$) (Naive) were analyzed as a reference. Data in (**A, B**) are from LAU1106. The corresponding dot graph shows the corresponding analysis from n=5 patients. Error bars are SD.

(**C-G**) Localization of TCF1$^+$ PD1$^+$ CD8+ T cells in melanoma tissues using multiplex immunohistochemistry (**C**) A representative composite image showing the presence of CD8$^+$ T cells (green) and tumor cells (brown). Dashed gray lines define the tumor area based on tissue segmentation and white rectangles depict areas shown in (**D**) at higher resolution. (**E-G**) Quantitative image analysis was used for (**E**) the segmentation of the tissue into tumor (grown), stroma (green) and acellular areas (blue), (**F**) single cell phenotype ma p distinguishing 6 different cell types highlighted at higher resolution in (**G**). Arrows and arrowheads highlight TCF1$^+$ PD1$^+$ and TCF1$^-$ PD1$^+$ CD8$^+$ T cells, respectively. Scale bars represent 100μm in (**C, E**) and 25μm in (**D**).

(H) ssRNAseq analysis of individual *CD8A*$^+$ melanoma TIL (Mel79) (Tirosh et al., 2016) were analyzed for *TCF7* and *PDCD1* expression. (**I**) Expression of genes associated with memory, effector

differentiation or exhaustion in individual *CD8A*$^{+}$ TIL in individual *CD8A*$^{+}$ melanoma TIL. See also Figure S7.

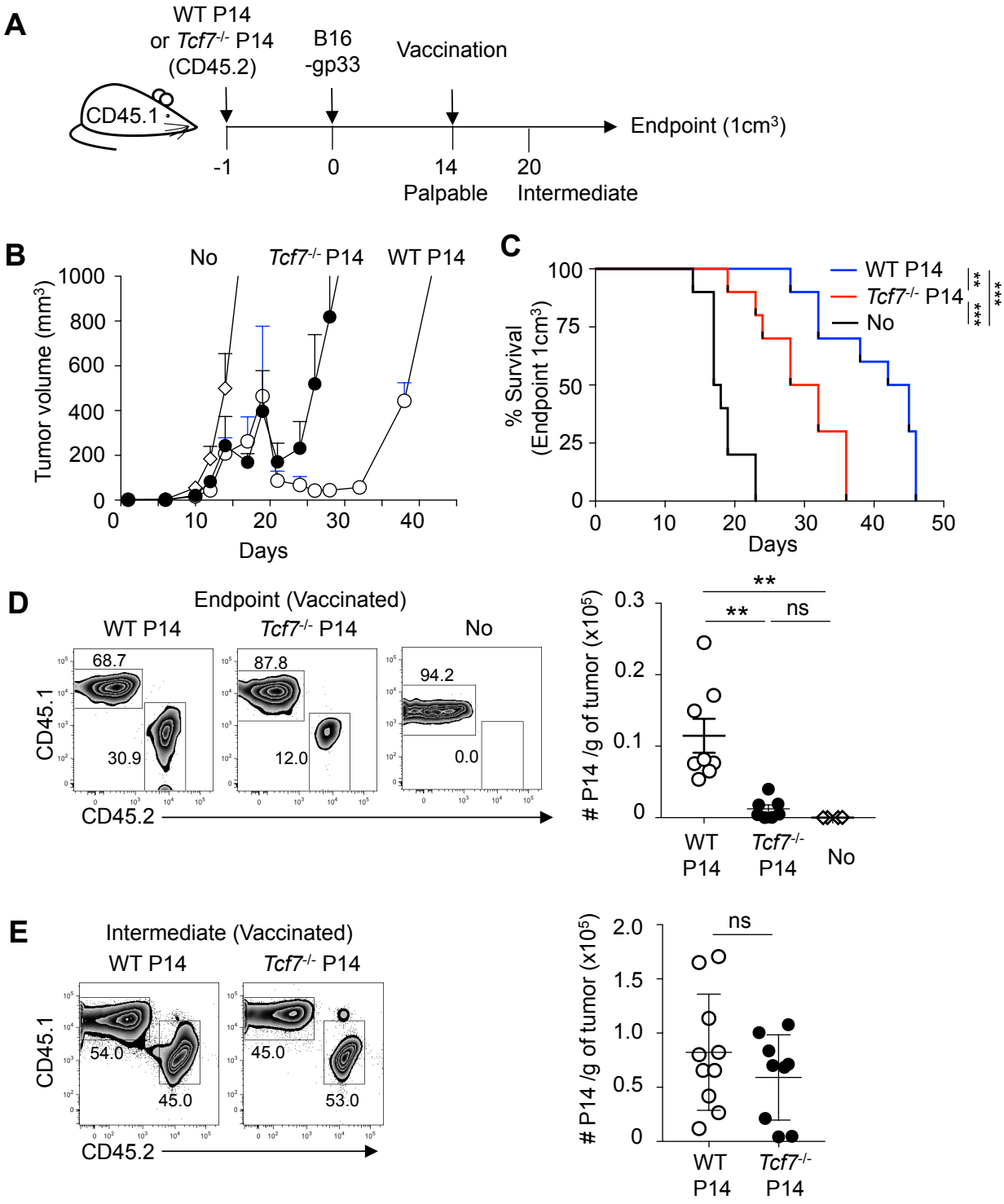
A
WT P14
or Tcf7-/- P14
(CD45.2)
B16
-gp33
Vaccination
CD45.1
Endpoint (1cm3)
-1
0
14
Palpable
20
Intermediate
B
No
Tcf7-/- P14
WT P14
Tumor volume (mm3)
Days
C
WT P14
Tcf7-/- P14
No
% Survival
(Endpoint 1cm3)
Days
D
Endpoint (Vaccinated)
WT P14
Tcf7-/- P14
No
68.7
30.9
87.8
12.0
94.2
0.0
CD45.1
CD45.2
P14 /g of tumor (x10^5)
ns
WT P14
Tcf7-/- P14
No
E
Intermediate (Vaccinated)
WT P14
Tcf7-/- P14
54.0
45.0
45.0
53.0
CD45.1
CD45.2
P14 /g of tumor (x10^5)
ns
WT P14
Tcf7-/- P14

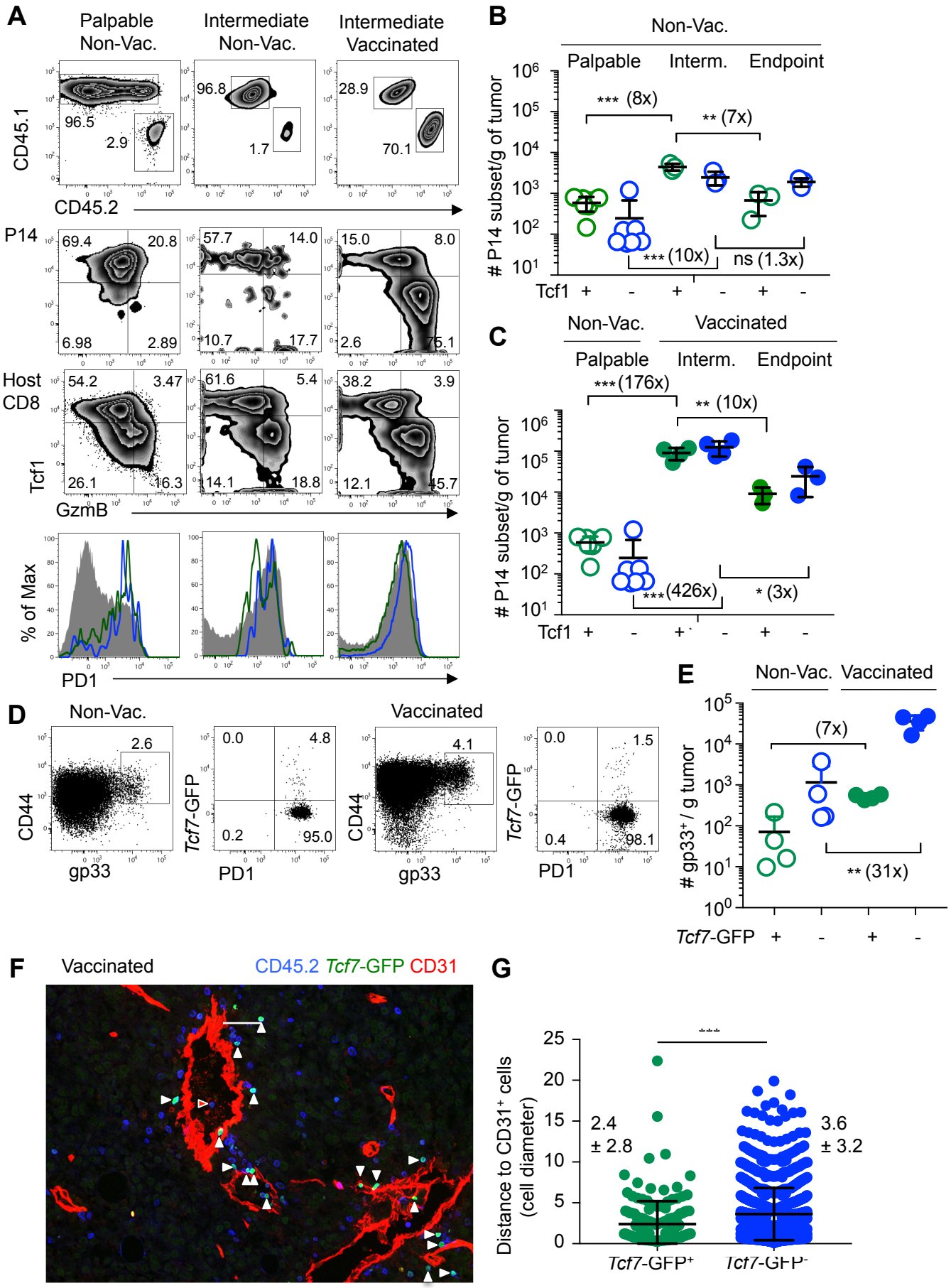
A
Palpable Non-Vac.
Intermediate Non-Vac.
Intermediate Vaccinated
CD45.1
CD45.2
96.5
2.9
96.8
1.7
28.9
70.1
P14
69.4
20.8
6.98
2.89
57.7
14.0
10.7
17.7
15.0
8.0
2.6
75.1
Host CD8
Tcf1
GzmB
54.2
3.47
26.1
16.3
61.6
5.4
14.1
18.8
38.2
3.9
12.1
45.7
% of Max
PD1
B
Non-Vac.
Palpable
Interm.
Endpoint
P14 subset/g of tumor
*** (8x)
** (7x)
*** (10x)
ns (1.3x)
Tcf1 + - + - + -
C
Non-Vac.
Vaccinated
Palpable
Interm.
Endpoint
***(176x)
** (10x)
***(426x)
* (3x)
# P14 subset/g of tumor
Tcf1 + - + - + -
D
Non-Vac.
Vaccinated
CD44
gp33
2.6
Tcf7-GFP
PD1
0.0
4.8
0.2
95.0
4.1
0.0
1.5
0.4
98.1
E
Non-Vac.
Vaccinated
(7x)
** (31x)
# gp33+ / g tumor
Tcf7-GFP + - + -
F
Vaccinated
CD45.2 Tcf7-GFP CD31
G
Distance to CD31+ cells (cell diameter)
2.4 ± 2.8
3.6 ± 3.2
Tcf7-GFP+
Tcf7-GFP-

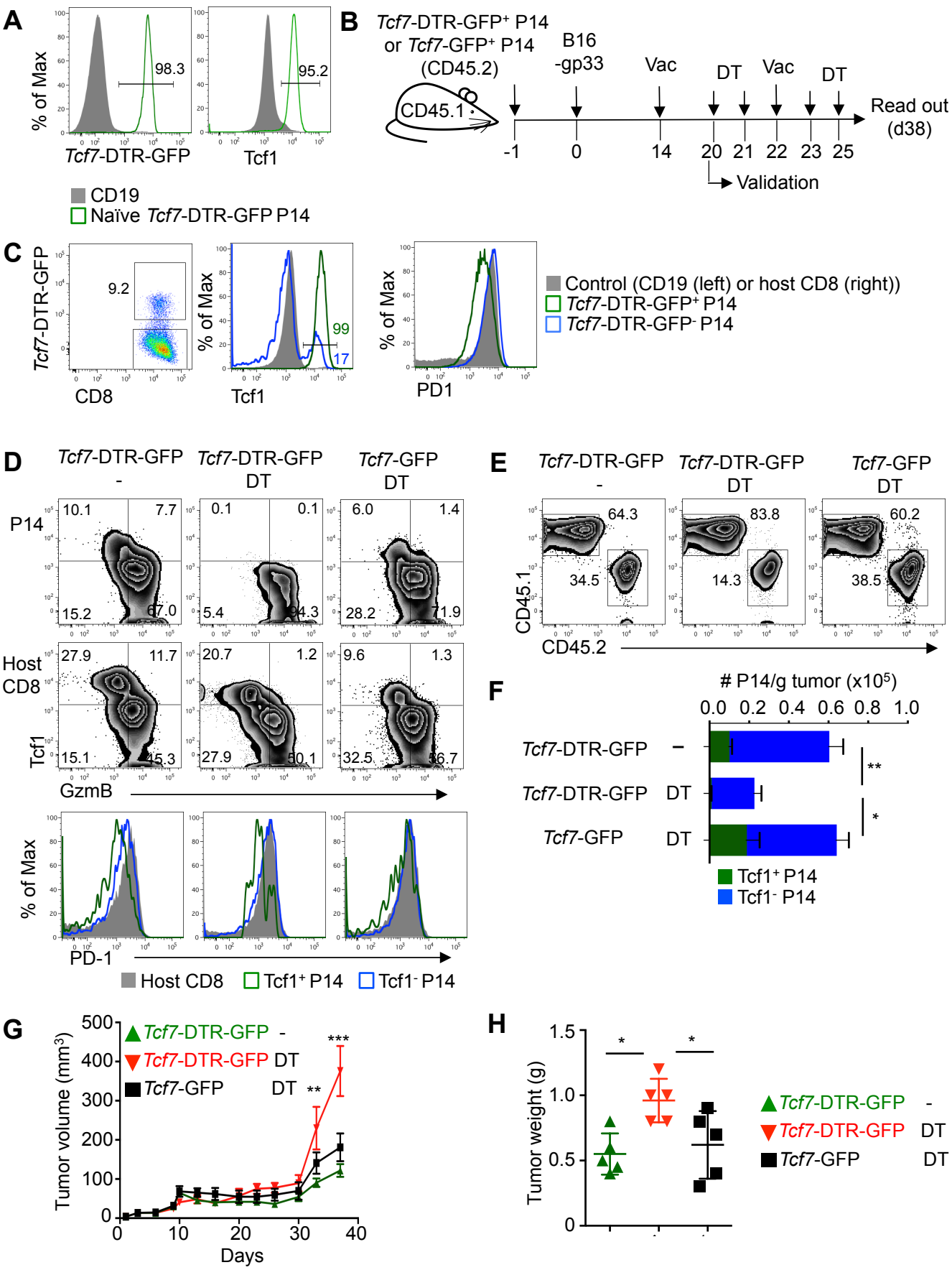
A
% of Max
98.3
95.2
Tcf7-DTR-GFP
Tcf1
CD19
Naïve Tcf7-DTR-GFP P14
B
Tcf7-DTR-GFP+ P14
or Tcf7-GFP+ P14
(CD45.2)
CD45.1
B16
-gp33
Vac
DT
Vac
DT
Read out
(d38)
-1
0
14
20
21
22
23
25
Validation
C
Tcf7-DTR-GFP
9.2
CD8
% of Max
99
17
Tcf1
% of Max
PD1
Control (CD19 (left) or host CD8 (right))
Tcf7-DTR-GFP+ P14
Tcf7-DTR-GFP- P14
D
Tcf7-DTR-GFP
-
Tcf7-DTR-GFP
DT
Tcf7-GFP
DT
P14
10.1
7.7
15.2
67.0
0.1
0.1
5.4
94.3
6.0
1.4
28.2
71.9
Host
CD8
27.9
11.7
15.1
45.3
20.7
1.2
27.9
50.1
9.6
1.3
32.5
56.7
Tcf1
GzmB
% of Max
PD-1
Host CD8
Tcf1+ P14
Tcf1- P14
E
Tcf7-DTR-GFP
-
Tcf7-DTR-GFP
DT
Tcf7-GFP
DT
64.3
34.5
83.8
14.3
60.2
38.5
CD45.1
CD45.2
F
P14/g tumor (x10^5)
0.0
0.2
0.4
0.6
0.8
1.0
Tcf7-DTR-GFP
-
Tcf7-DTR-GFP
DT
Tcf7-GFP
DT
**
*
Tcf1+ P14
Tcf1- P14
G
Tumor volume (mm3)
500
400
300
200
100
0
Tcf7-DTR-GFP -
Tcf7-DTR-GFP DT
Tcf7-GFP DT
***
**
0
10
20
30
40
Days
H
Tumor weight (g)
1.5
1.0
0.5
0
*
*
Tcf7-DTR-GFP -
Tcf7-DTR-GFP DT
Tcf7-GFP DT

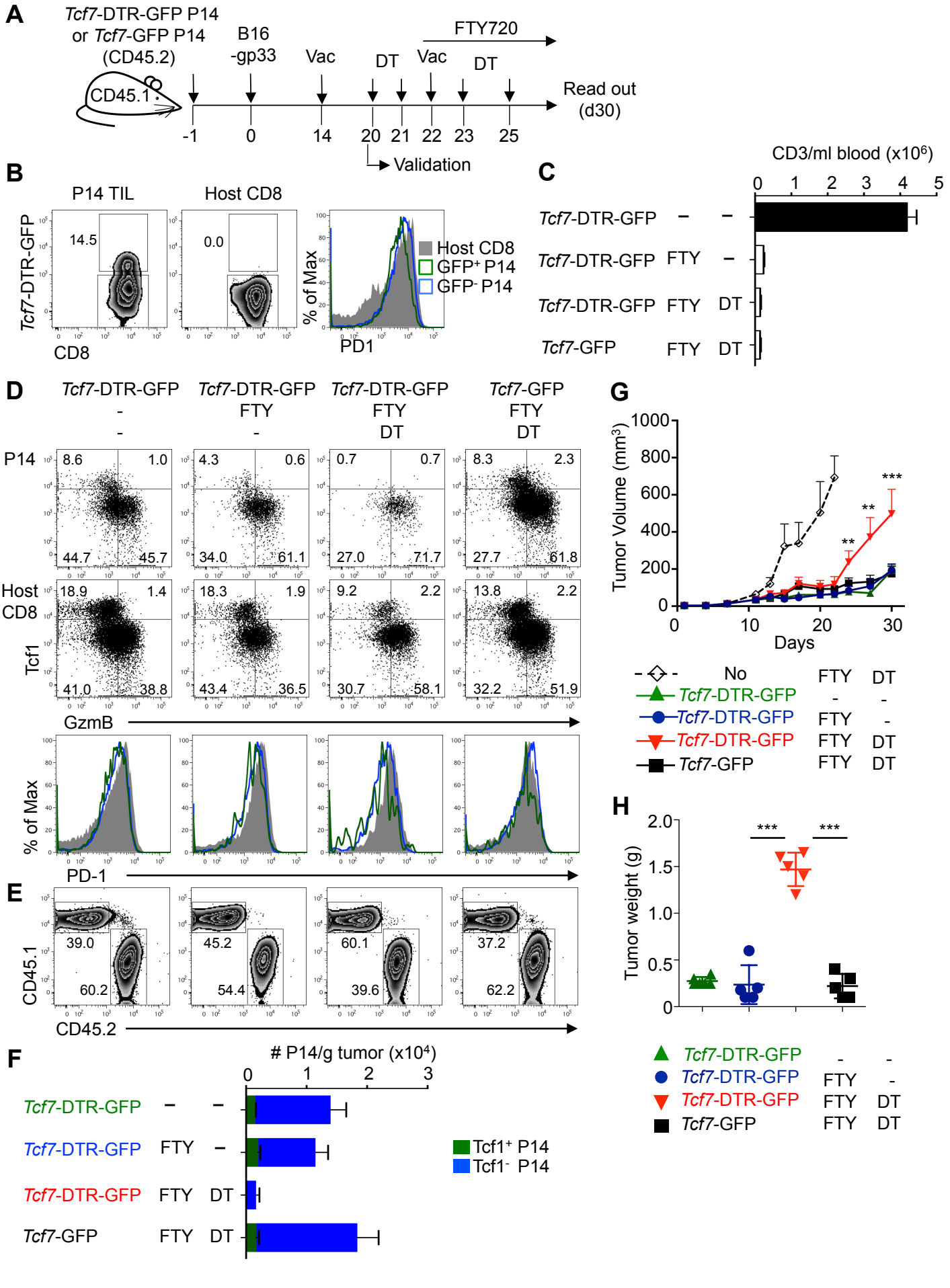
A
Tcf7-DTR-GFP P14
or Tcf7-GFP P14
(CD45.2)
CD45.1
B16
-gp33
Vac
DT
Vac
DT
FTY720
Read out
(d30)
-1
0
14
20
21
22
23
25
Validation
B
P14 TIL
Host CD8
Tcf7-DTR-GFP
14.5
0.0
CD8
% of Max
PD1
Host CD8
GFP+ P14
GFP- P14
C
CD3/ml blood (x10^6)
0
1
2
3
4
5
Tcf7-DTR-GFP - -
Tcf7-DTR-GFP FTY -
Tcf7-DTR-GFP FTY DT
Tcf7-GFP FTY DT
D
Tcf7-DTR-GFP - -
Tcf7-DTR-GFP FTY -
Tcf7-DTR-GFP FTY DT
Tcf7-GFP FTY DT
P14
8.6
1.0
44.7
45.7
4.3
0.6
34.0
61.1
0.7
0.7
27.0
71.7
8.3
2.3
27.7
61.8
Host CD8
Tcf1
18.9
1.4
41.0
38.8
18.3
1.9
43.4
36.5
9.2
2.2
30.7
58.1
13.8
2.2
32.2
51.9
GzmB
% of Max
PD-1
E
CD45.1
39.0
60.2
45.2
54.4
60.1
39.6
37.2
62.2
CD45.2
F
P14/g tumor (x10^4)
0
1
2
3
Tcf7-DTR-GFP - -
Tcf7-DTR-GFP FTY -
Tcf7-DTR-GFP FTY DT
Tcf7-GFP FTY DT
Tcf1+ P14
Tcf1- P14
G
Tumor Volume (mm3)
1000
800
600
400
200
0
0
10
20
30
Days
**
**
***
No FTY DT
Tcf7-DTR-GFP - -
Tcf7-DTR-GFP FTY -
Tcf7-DTR-GFP FTY DT
Tcf7-GFP FTY DT
H
Tumor weight (g)
2.0
1.5
1.0
0.5
0
***
***
Tcf7-DTR-GFP - -
Tcf7-DTR-GFP FTY -
Tcf7-DTR-GFP FTY DT
Tcf7-GFP FTY DT

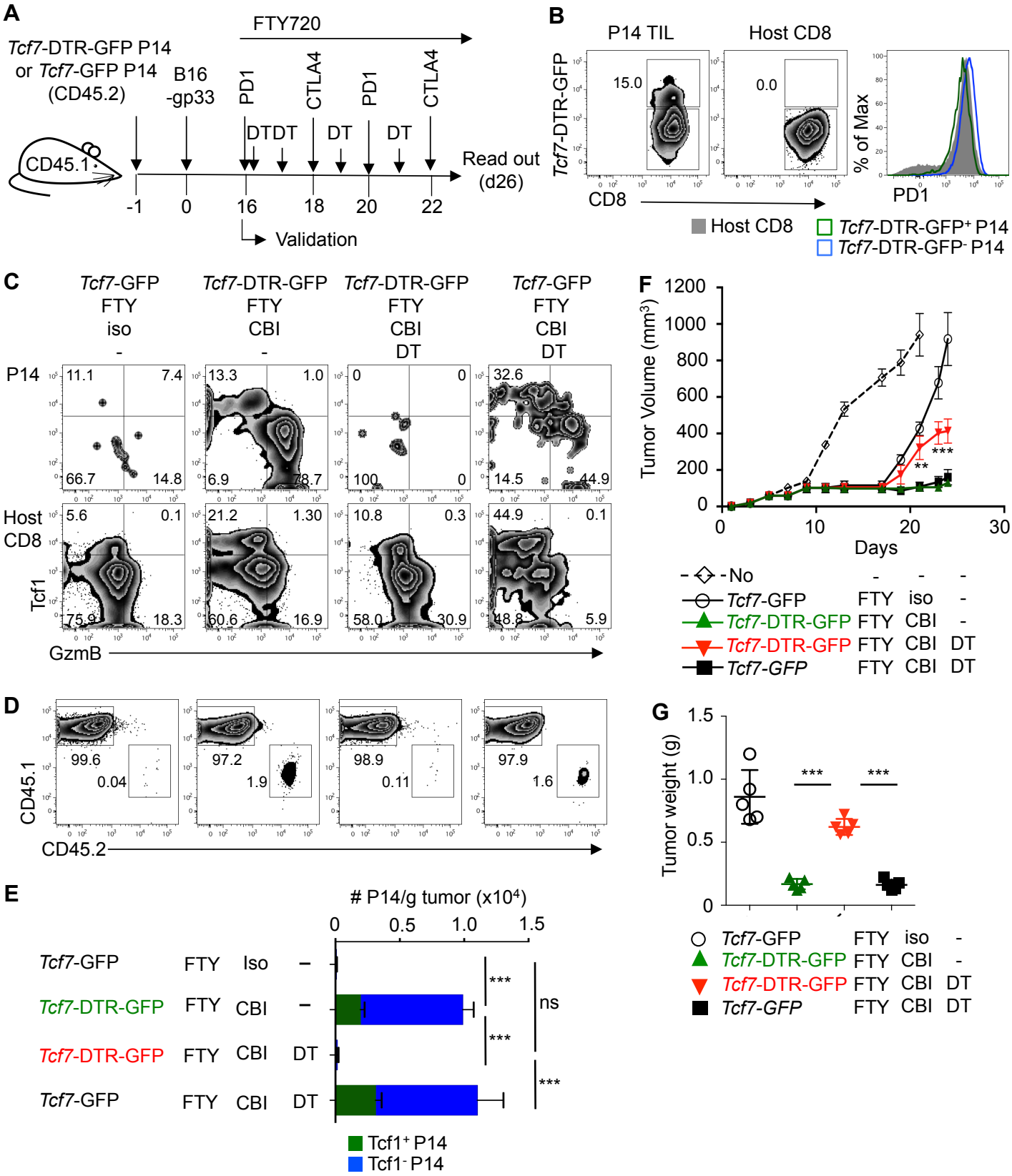
A
FTY720
Tcf7-DTR-GFP P14
or Tcf7-GFP P14
(CD45.2)
B16
-gp33
PD1
CTLA4
PD1
CTLA4
DTDT
DT
DT
CD45.1
Read out
(d26)
-1
0
16
18
20
22
Validation
B
P14 TIL
Host CD8
Tcf7-DTR-GFP
15.0
0.0
CD8
% of Max
PD1
Host CD8
Tcf7-DTR-GFP+ P14
Tcf7-DTR-GFP- P14
C
Tcf7-GFP FTY iso -
Tcf7-DTR-GFP FTY CBI -
Tcf7-DTR-GFP FTY CBI DT
Tcf7-GFP FTY CBI DT
P14
11.1
7.4
66.7
14.8
13.3
1.0
6.9
78.7
0
0
100
0
32.6
14.5
44.9
Host CD8
Tcf1
5.6
0.1
75.9
18.3
21.2
1.30
60.6
16.9
10.8
0.3
58.0
30.9
44.9
0.1
48.8
5.9
GzmB
F
Tumor Volume (mm3)
1200
1000
800
600
400
200
0
0
10
20
30
Days
***
**
No - - -
Tcf7-GFP FTY iso -
Tcf7-DTR-GFP FTY CBI -
Tcf7-DTR-GFP FTY CBI DT
Tcf7-GFP FTY CBI DT
D
CD45.1
99.6
0.04
97.2
1.9
98.9
0.11
97.9
1.6
CD45.2
G
Tumor weight (g)
1.5
1.0
0.5
0
***
***
Tcf7-GFP FTY iso -
Tcf7-DTR-GFP FTY CBI -
Tcf7-DTR-GFP FTY CBI DT
Tcf7-GFP FTY CBI DT
E
P14/g tumor (x10⁴)
0
0.5
1.0
1.5
Tcf7-GFP FTY Iso –
Tcf7-DTR-GFP FTY CBI –
Tcf7-DTR-GFP FTY CBI DT
Tcf7-GFP FTY CBI DT
***
***
***
ns
Tcf1+ P14
Tcf1- P14

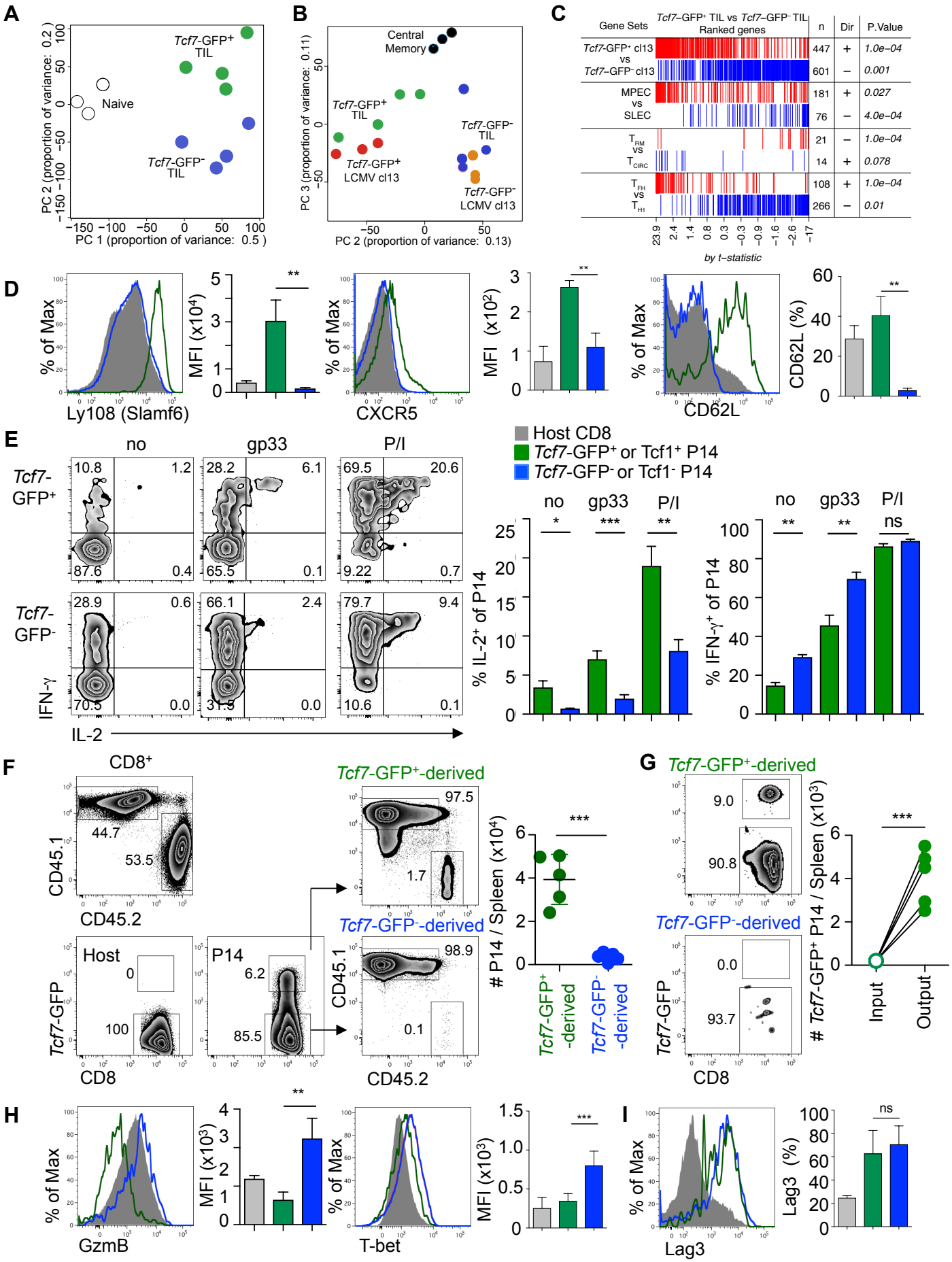
A
PC 2 (proportion of variance: 0.2)
PC 1 (proportion of variance: 0.5)
Tcf7-GFP+ TIL
Naive
Tcf7-GFP- TIL
B
PC 3 (proportion of variance: 0.11)
PC 2 (proportion of variance: 0.13)
Central Memory
Tcf7-GFP+ TIL
Tcf7-GFP+ LCMV cl13
Tcf7-GFP- TIL
Tcf7-GFP- LCMV cl13
C
Gene Sets
Tcf7–GFP+ TIL vs Tcf7–GFP- TIL Ranked genes
n
Dir
P.Value
Tcf7-GFP+ cl13 vs Tcf7-GFP- cl13
447 + 1.0e–04
601 – 0.001
MPEC vs SLEC
181 + 0.027
76 – 4.0e–04
T_RM vs T_CIRC
21 – 1.0e–04
14 + 0.078
T_FH vs T_H1
108 + 1.0e–04
266 – 0.01
by t–statistic
D
% of Max
Ly108 (Slamf6)
MFI (x10^4)
CXCR5
MFI (x10^2)
CD62L
CD62L (%)
E
no
gp33
P/I
Tcf7-GFP+
Tcf7-GFP-
IFN-γ
IL-2
Host CD8
Tcf7-GFP+ or Tcf1+ P14
Tcf7-GFP- or Tcf1- P14
% IL-2+ of P14
% IFN-γ+ of P14
ns
F
CD8+
CD45.1
CD45.2
Tcf7-GFP+-derived
Tcf7-GFP--derived
Host
P14
Tcf7-GFP
CD8
P14 / Spleen (x10^4)
G
Tcf7-GFP+-derived
Tcf7-GFP--derived
Tcf7-GFP+ P14 / Spleen (x10^3)
Input
Output
H
GzmB
T-bet
I
Lag3
Lag3 (%)

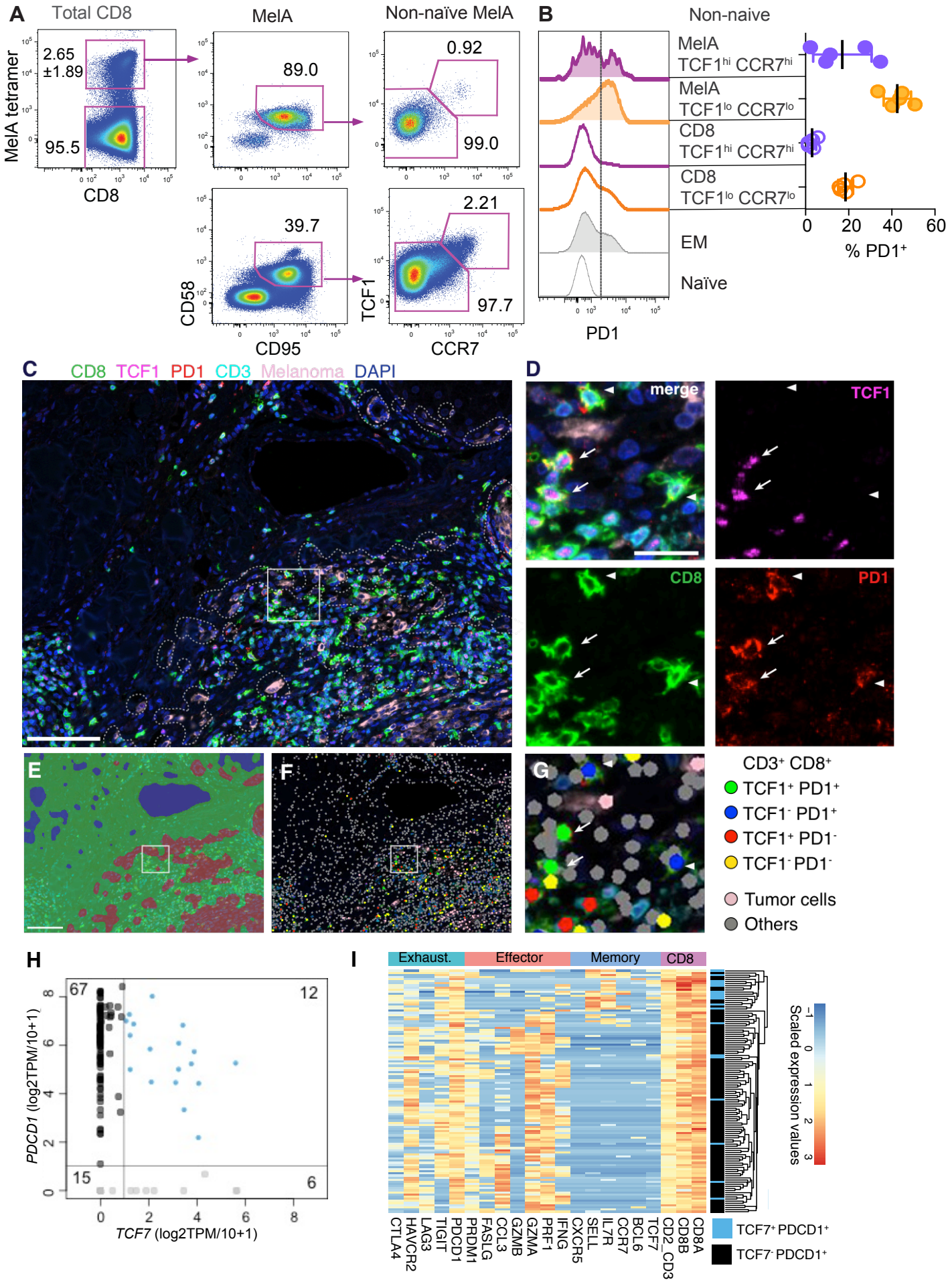
A
Total CD8
MelA
Non-naïve MelA
MelA tetramer
2.65
±1.89
95.5
CD8
89.0
0.92
99.0
39.7
2.21
97.7
CD58
CD95
TCF1
CCR7
B
Non-naive
MelA
TCF1hi CCR7hi
MelA
TCF1lo CCR7lo
CD8
TCF1hi CCR7hi
CD8
TCF1lo CCR7lo
EM
Naïve
PD1
0
20
40
60
% PD1+
C
CD8 TCF1 PD1 CD3 Melanoma DAPI
D
merge
TCF1
CD8
PD1
E
F
G
CD3+ CD8+
TCF1+ PD1+
TCF1- PD1+
TCF1+ PD1-
TCF1- PD1-
Tumor cells
Others
H
67
12
15
6
PDCD1 (log2TPM/10+1)
TCF7 (log2TPM/10+1)
I
Exhaust.
Effector
Memory
CD8
CTLA4
HAVCR2
LAG3
TIGIT
PDCD1
PRDM1
FASLG
CCL3
GZMB
GZMA
PRF1
IFNG
CXCR5
SELL
IL7R
CCR7
BCL6
TCF7
CD2_CD3
CD8B
CD8A
Scaled expression values
TCF7+ PDCD1+
TCF7- PDCD1+

Supplemental Figure 1

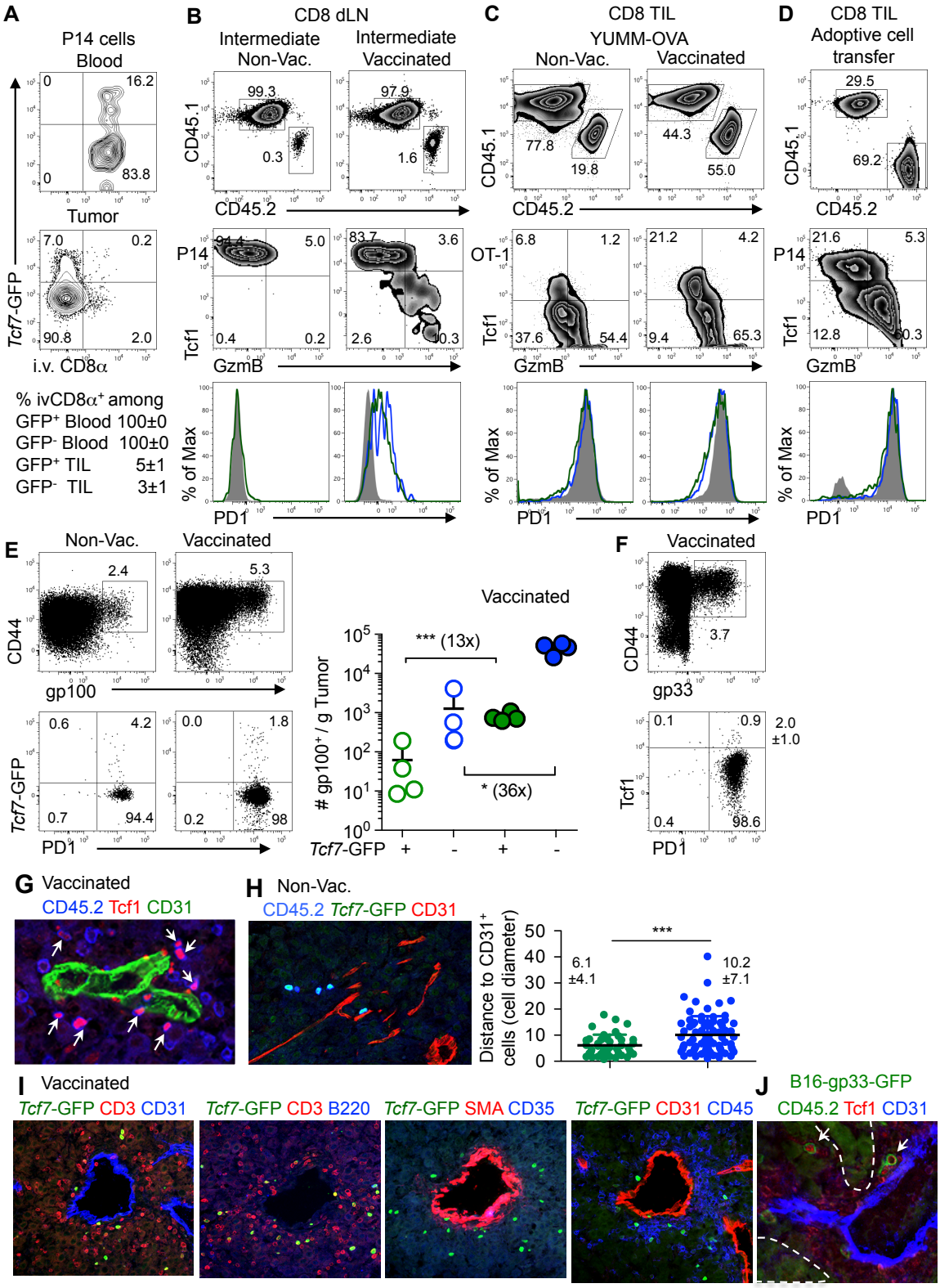

Figure S1. Tumor-specific CD8 T cells harbor prominent Tcf1$^+$ PD1$^+$ GzmB$^-$ and Tcf1$^-$ PD1$^+$ GzmB$^+$ subsets. Related to Figure 2.

(**A**) B6 mice (CD45.1) were grafted with *Tcf7*-GFP P14 cells (CD45.2) and implanted s.c. with B16-gp33 tumor cells one day later. Mice were vaccinated with gp33/polyIC when tumors became palpable. One week after vaccination tumor bearing mice were injected i.v. with fluorescent CD8a antibody (i.v. CD8α) before sacrifice. Blood borne and tumor-associated P14 cells were analyzed for their exposure to the i.v. CD8α mAb. Data are compiled from 2 independent experiments, n=6 mice total.

(**B**) B6 mice (CD45.1) were grafted with WT P14 cells (CD45.2) and implanted s.c. with B16-gp33 tumor cells one day later. Mice were left untreated and analyzed when the tumor had an intermediate size or mice were vaccinated with gp33/polyIC when tumors became palpable and analyzed one week later. Tumor draining LN were were analyzed for the presence of P14 cells ($CD45.2^+$). Density plots show Tcf1 versus GzmB expression in gated P14 cells (CD45.2). Histogram overlays show PD1 expression in gated $Tcf1^+$ P14 cells (green), $Tcf1^-$ P14 cells (blue) as compared to host CD8 T cells (grey fill). Data are representative of 2 independent experiments with n= 5 mice per group.
(**C**) Analysis of TIL derived from YUMM-OVA melanoma. B6 mice (CD45.2) were engrafted with OT-I T cells (CD45.1) and implanted s.c. with YUMM-OVA melanoma cells. Recipients were left untreated or vaccinated with Ova/polyIC when tumors became palpable and all mice were analyzed 6 days later. Density plots (top) show the abundance of OT-I cells (CD45.1) Top) and Tcf1 versus GzmB expression in gated OT-I cells (middle). Histogram overlays show PD1 expression in gated $Tcf1^+$ $GzmB^-$ P14 cells (green), $Tcf1^-$ $GzmB^+$ P14 cells (blue) as compared to host CD8 T cells (grey fill). Data are representative of a single experiments with n=5 mice per group.
(**D**) Adoptive T cell transfer: B6 mice (CD45.1) implanted with B16-gp33 tumor cells were sublethally irradiated when tumors became palpable. One day later mice were grafted with *in vitro* activated P14 cells. CD8 TIL were analyzed 10 days later for the presence of P14 cells and for the expression of Tcf1 versus GzmB or PD1. Data are representative of 2 independent experiments with a total of n=6 mice.
(**E, F**) Presence of $Tcf1^+$ $PD1^+$ cells amongst polyclonal CD8 TIL. *Tcf*7-GFP reporter mice were implanted with B16-gp33 tumor cells. Mice were either left untreated or were vaccinated with a mixture of gp33, gp100 and Trp2 peptides plus polyI:C when tumors became palpable. TIL were analyzed one week later. (**E**) Density plots show gated CD8 TIL stained for CD44 versus gp100 tetramer (gp100) (left) and $gp100^+$ CD8 TIL were analyzed for *Tcf*7-GFP and PD1 expression (right). The dot graph depicts the abundance of *Tcf*7-GFP^+ $gp100^+$ TIL (green) versus *Tcf*7-GFP^- $gp100^+$ TIL (blue) per gram of tumor in untreated mice (open circles) versus vaccinated mice (filled circles). Data are representative of 2 independent experiments with n=3-5 mice per group. (**F**) Tcf1 expressing $gp33^+$ CD8 T cells in vaccinated mice were also detected using Tcf1 protein expression. Data are from a single independent experiments with n=4 mice.
(**G-J**) Immuno localization of P14 TIL subsets in B16-gp33 tumors. (**G**) *Tcf*7-GFP P14 chimeric mice were implanted with B16-gp33 tumor cells and mice were vaccinated with gp33/polyIC when tumors became palpable. One week later, B16-gp33 tumor sections were analyzed for the presence of P14 cells (CD45.2) (blue), Tcf1 protein (red) and endothelial cells (CD31) (green). (**H**) B16-gp33 tumor tissue in non-vaccinated mice was analyzed for P14 cells (CD45.2) (blue), *Tcf*7-GFP (green) and endothelial cells (CD31) (red). The dot graph shows the mean distance (±SD) (in lymphocyte diameters) between endothelial cells ($CD31^+$) and individual *Tcf*7-GFP^+ $CD45.2^+$ or *Tcf*7-GFP^- $CD45.2^+$ cells (n=78). (**I**) B16-gp33 tumor tissue in vaccinated mice was analyzed for the localization of *Tcf*7-GFP^+ cells (green) relative to T cells (CD3), B cells (B220), hematopoietic cells (CD45), endothelial cells (CD31, Smooth Muscle Actin (SMA)) and Follicular Dendritic Cells (FDC) (CD35). (**J**) B16-gp33-GFP^+ tumor tissue in vaccinated mice was analyzed for P14 cells (CD45.2) (green), Tcf1 protein (red) and endothelial cells (CD31) (blue).
Data in (**G-J)** are representative of 2 independent experiments with 2 mice per group. Error bars in (**E, H**) are SD and statistics is based on unpaired t-test

Supplemental Figure 2

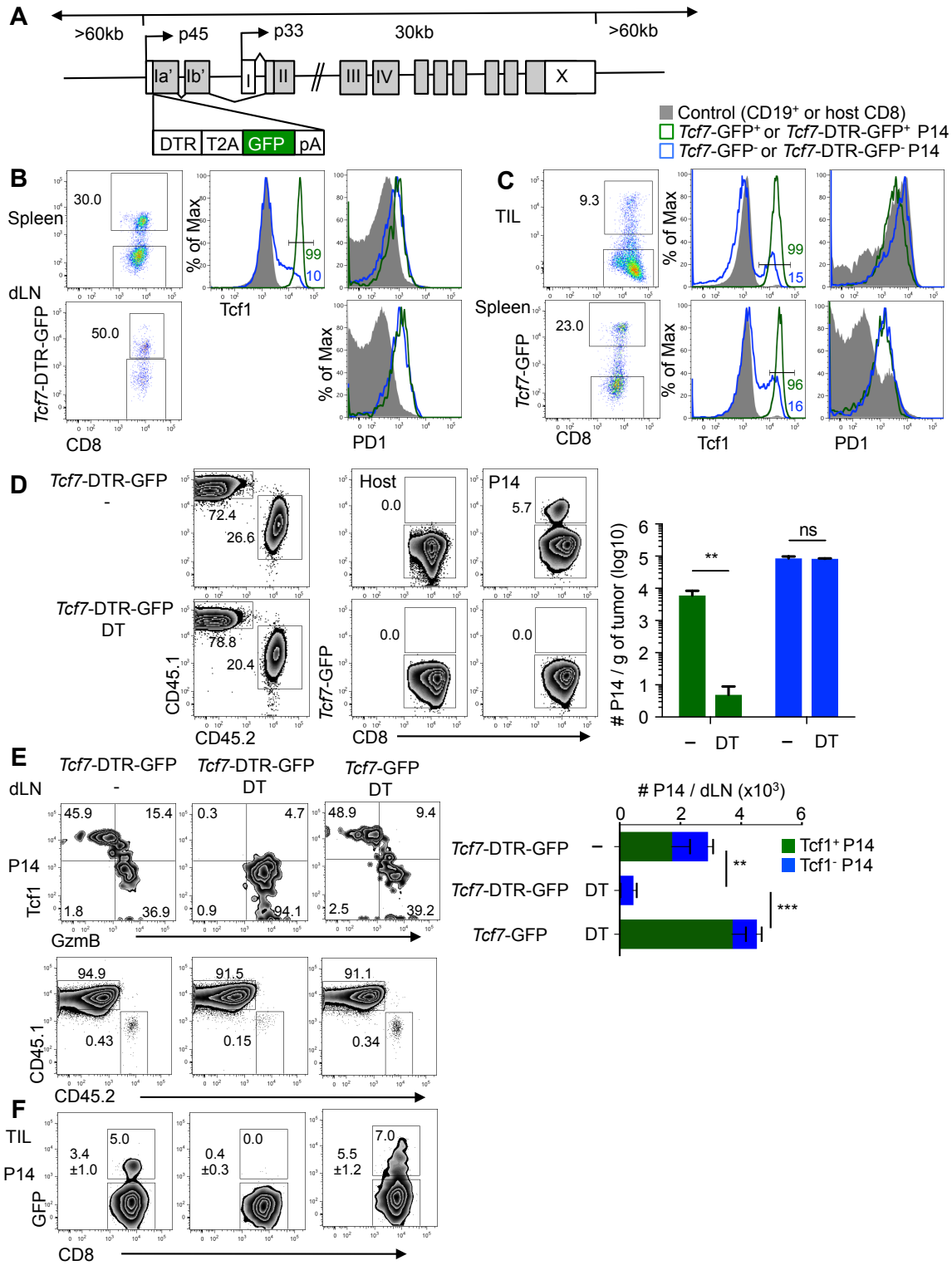

Figure S2. Extended tumor control following therapeutic vaccination depends on tumor-specific Tcf1$^+$ CD8 T cells. Related to Figure 4.

(**A**) Schematic representation of the *Tcf7*-DTR-GFP construct. A diphtheria toxin receptor (DTR) T2A green fluorescent protein (GFP) fusion gene was inserted into the first exon of the *Tcf7* locus present on a > 150kb BAC, which was used to generate *Tcf7*-DTR-GFP transgenic mice.

(**B, C**) *Tcf7*-DTR-GFP or *Tcf7*-GFP P14 chimeric B16-gp33 tumor bearing mice were vaccinated when tumors became palpable and analyzed 6 days later. (**B**) Density plots show GFP expression in *Tcf7*-DTR-GFP P14 cells present in the spleen (top) or dLN (bottom). The histogram overlay (center) shows Tcf1 protein expression in

flow sorted *Tcf*7-DTR-GFP$^+$ (green) and *Tcf*7-DTR-GFP$^-$ P14 cells (blue) present in the spleen (left). Histogram overlays (right) show PD1 expression in *Tcf*7-DTR-GFP$^+$ (green) and *Tcf*7-DTR-GFP$^-$ (blue) P14 cell present in the spleen (right top) or the dLN (bottom). (**C**) Same validation as in (**B)** but for *Tcf*7-GFP P14 cells amongst TIL (top) or in the spleen (bottom).

(**D)** *Tcf*7-DTR-GFP P14 chimeric, B16-gp33 tumor bearing mice were vaccinated and injected with diphtheria toxin (DT) on day 6 and 7 post vaccination and analyzed one day later. Density plots show the abundance of total P14 cells and the presence of *Tcf*7-DTR-GFP$^+$ P14 TIL. The bar graph shows the abundance of *Tcf*7-DTR-GFP$^+$ (green) and *Tcf*7-DTR-GFP$^-$ (blue) P14 cells per g of tumor.

(**E, F**) Analysis of tumor bearing mice following DT-mediated ablation of *Tcf*7-DTR-GFP$^+$ P14 cells. (**E**) Density plots show dLN analyzed for the expression of Tcf1 versus GzmB expression in *Tcf*7-DTR-GFP or Tcf7-GFP P14 cells (CD45.2$^+$) (top) and the abundance of P14 cells (bottom). The bar graph depicts the mean number (±SD) of Tcf1$^+$ P14 (green) and Tcf1$^-$ P14 cells (blue) in the dLN. (**F**) Density plots show gated P14 (CD45.2) analyzed for the expression of GFP.

Data in (**B**, **C**) are representative of 2 independent experiments, in (**D**) are representative of two independent experiments with n=2-4 mice per group (**E**) are representative of 2 independent experiments each with n=5 mice per group. Error bars (**D, E**) are SD. Statistics is based on unpaired t-test in (**D**) or one-way Anova in (**G**).

Supplemental Figure 3

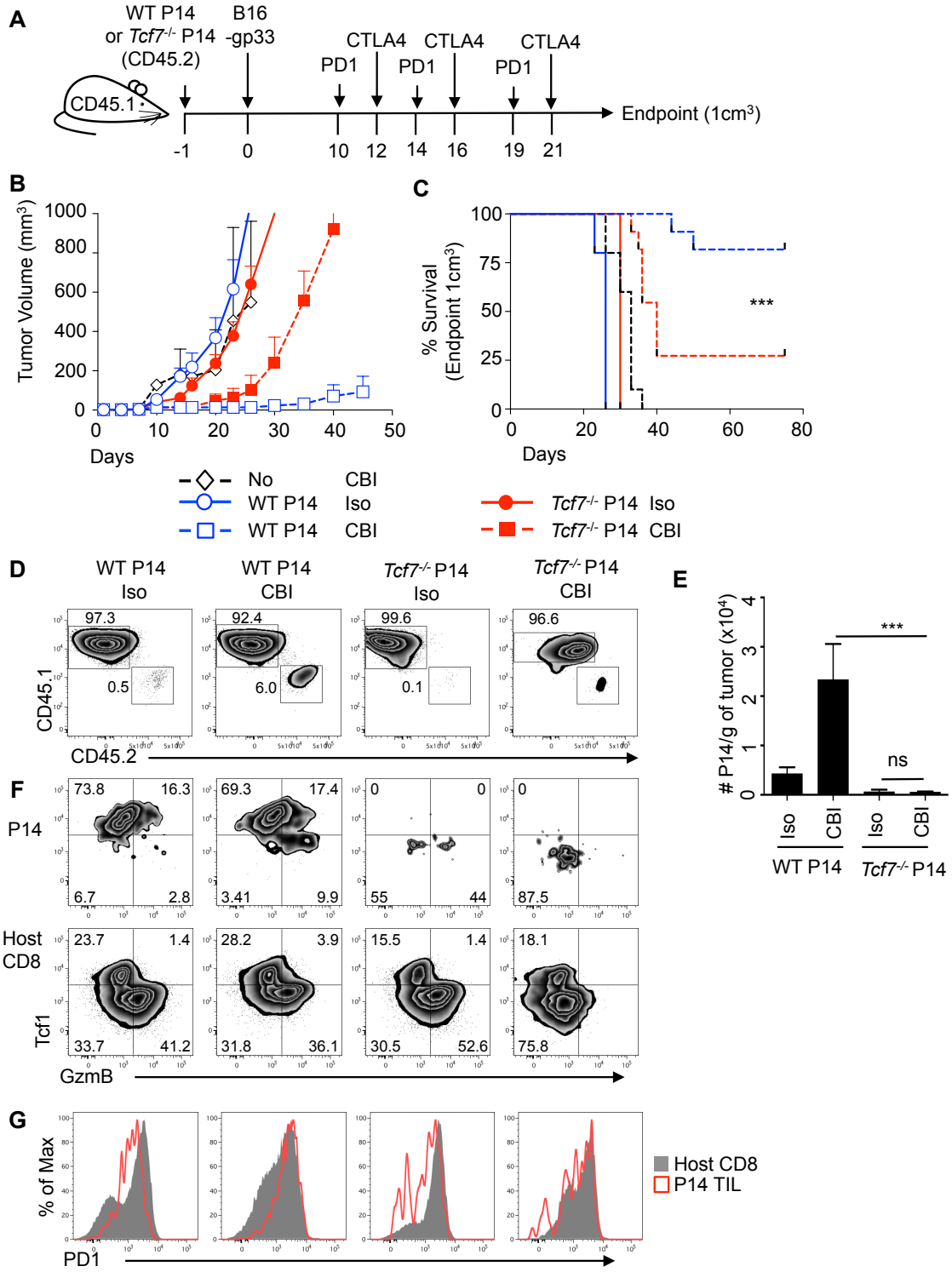

Figure S3. Checkpoint blockade leads to long-term tumor protection in the presence of tumor-specific *Tcf7*$^{+/+}$ CD8 T cells. Related to Figure 5.

(**A-G**) WT or *Tcf7*$^{-/-}$ P14 chimeric mice were implanted s.c. with B16-gp33 tumor cells. When tumors became palpable, mice were treated with anti-PD1/CTLA4 (checkpoint blockade immunotherapy (CBI)) or isotype control Ab according to the indicated regimen. (**B**) B16-gp33 tumor volume in mice harboring WT or *Tcf7*$^{-/-}$ P14 T cells or no P14 cells (No) and treated with anti-PD1/CTLA-4 (CBI) or isotype. (**C**) Plot depicting the fraction of mice with a tumor <1cm^3. (**D**) Density plots show gated CD8 TIL analyzed for the presence of P14 TIL (CD45.2). (**E**) The corresponding bar graph depicts the mean number (±SD) of P14 TIL per g of tumor. (**F**)

Density plots show gated P14 TIL (top) and host CD8 TIL (bottom) analyzed for the expression of Tcf1 versus GzmB. (**G**) Histogram overlays show PD1 expression in P14 TIL (red) as compared to host CD8 TIL (grey fill). Data in (**B, D-G**) are representative of 2 independent experiments, most groups with n=5 mice in each experiment. Data in (**C**) are compiled from 2 independent experiments with a total of n=5-11 mice per group. Error bars are SEM in (**B**) and SD in (**E**). Statistics: ***$p<0.001$; ns=not significant ($p>0.05$) based on log rank test (**C**) or one-way Anova (**E**).

Supplemental Figure 4

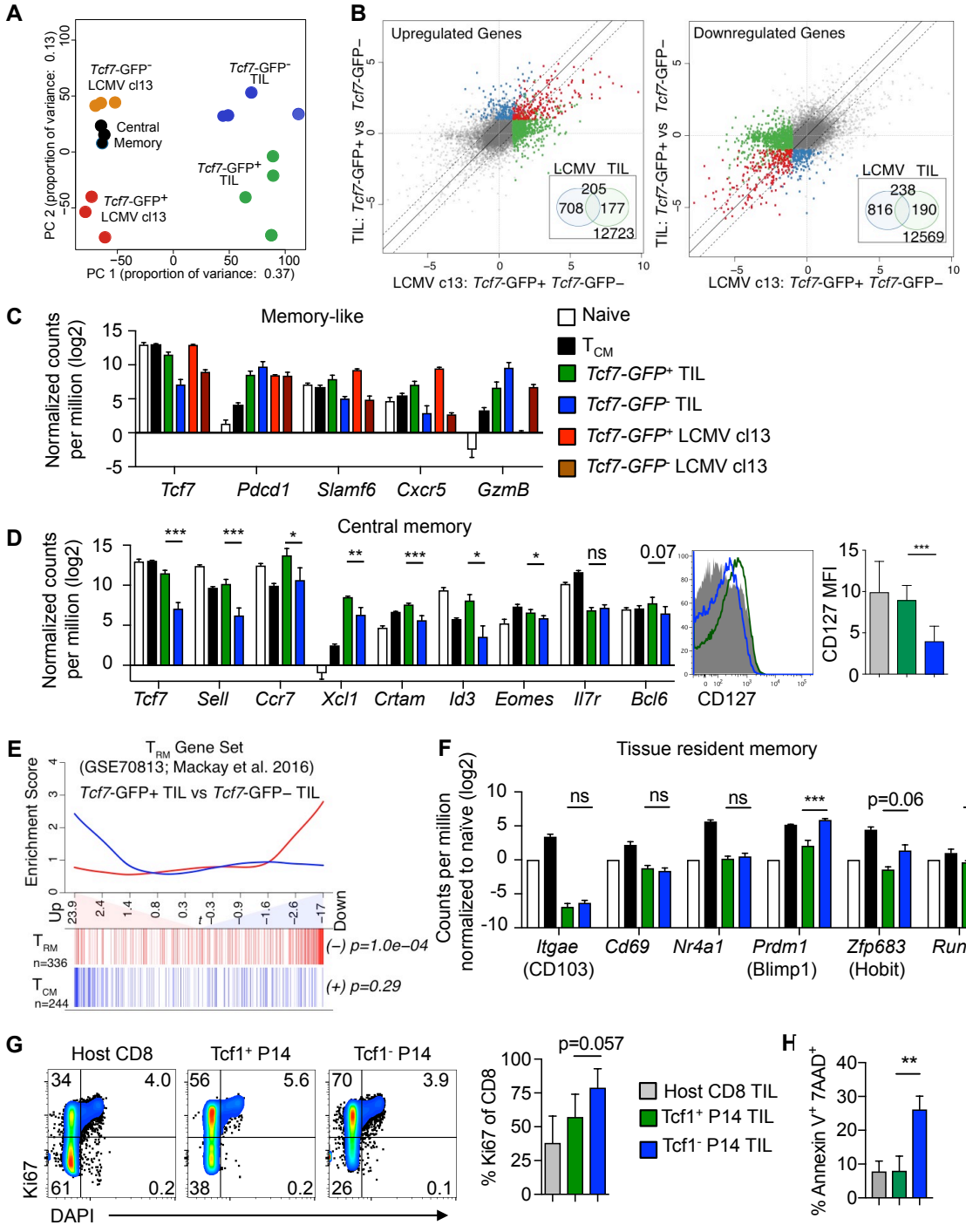

Figure S4. Tumor-specific Tcf1$^+$ PD1$^+$ CD8 TIL combine features of exhausted cells and stem-like properties. Related to Figure 6:

Tcf7-GFP$^+$ P14 chimeric mice were implanted with B16-gp33 tumors cells and one vaccinated when tumors became palpable. One week later *Tcf7*-GFP$^+$ and *Tcf7*-GFP$^-$ P14 TIL were flow sorted and subjected to gene expression analysis using RNA-seq. **(A)** Principal component analysis (PCA) of tumor-derived P14 cells (*Tcf7*-GFP$^+$ TIL and *Tcf7*-GFP$^-$ TIL, respectively) in conjunction with P14 cells derived from chronic LCMV infection (*Tcf7*-GFP$^+$ LCMV cl13 and *Tcf7*-GFP$^-$ LCMV cl13) or *Tcf7*-GFP$^+$ P14 cells derived from acute-resolved LCMV infection (Central memory) (Utzschneider et al., 2016). Data correction was based on the transcriptomes of naive P14 cells, which were analyzed in both experiments. PC1 vs PC2 separated cells derived from tumors and those derived from viral infections.

(**B**) Data from TIL and chronic viral infection were analyzed separately to identify genes differentially expressed between *Tcf7*-GFP$^+$ TIL and *Tcf7*-GFP$^-$ TIL and between *Tcf7*-GFP$^+$ LCMV cl13 and *Tcf7*-GFP$^-$ LCMV cl13

P14 cells (FDR<5% and FC>2). The dot plot depicts genes that are upregulated in *Tcf7*-GFP$^+$ TIL as well as *Tcf7*-GFP$^+$ LCMV cl13 P14 cells (red dots) or that are specifically upregulated in *Tcf7*-GFP$^+$ TIL (blue) or in *Tcf7*-GFP$^+$ LCMV cl13 P14 cells (green). The same analysis was performed for downregulated genes (right)

(**C**) The bar graph shows the expression of selected genes associated with memory-like CD8 T cell phenotype in naive CD8 T cells (Naive), central memory (T_{CM}) cells, in *Tcf7*-GFP$^+$ and *Tcf7*-GFP$^-$ cells derived from tumors (TIL) or chronic viral infection (LCMV cl13). The RNAseq data shown herein and from (Utzschnieder et al 2016) were combined using naive CD8 T cells for normalization.

(**D**) The bar graph shows the expression of selected genes associated with central memory in naive CD8 T cells (Naive), central memory (T_{CM}) cells and in *Tcf7*-GFP$^+$ and *Tcf7*-GFP$^-$ cells derived from tumors (TIL). The histogram overlays shows the expression of CD127 (IL7Ra) in *Tcf7*-GFP$^+$ TIL (green), *Tcf7*-GFP$^-$ TIL (blue) as compared to host CD8 TIL (grey fill). The corresponding bar graph depicts the mean fluorescence intensity (MFI) of staining.

(**E**) Gene set enrichment tests of tissue resident memory cells (T_{RM}) versus central memory cells (T_{CM}) (Mackay et al., 2016) over the *Tcf7*-GFP$^+$ TIL versus *Tcf7*-GFP$^-$ TIL comparison ranked by the t-statistic.

(**F**) The bar graph shows the expression of selected genes associated with tissue resident memory cells in naive CD8 T cells (Naive), tissue resident memory cells (T_{RM}) cells and in *Tcf7*-GFP$^+$ and *Tcf7*-GFP$^-$ cells derived from tumors (TIL). RNAseq data from (Mackay et al., 2016) and from the present study were normalized for each gene using naive CD8 T cells (= 1.0).

(**G**) Density plots show the expression of Ki67 versus DAPI in gated Tcf1$^+$ and Tcf1$^-$ P14 TIL. The bar graph shows the percentage of Ki67$^+$ cells in the indicated population.

(**H**) TIL were cultured for 4 h in the absence of growth factors before staining with Annexin V and 7-AAD. The bar graph shows the abundance of AnnexinV$^+$ 7-AAD$^+$ cells of gated *Tcf7*-GFP$^+$ (green) and Tcf7-GFP$^-$ P14 TIL (blue).

Data in (**A-F**) are normalized counts derived from RNAseq analysis of n=3-4 independent samples per group. The data from the (Mackay et al., 2016) study are duplicates **(E-F**). Data in (**G**) are representative of 2 independent experiments with n=4 and 5 mice. Data in (**H**) are representative of 2 independent experiment with n=3 and 4 mice. All error bars are SD. Statistics in (**G, H**) is based on unpaired t-test.

Supplemental Figure 5

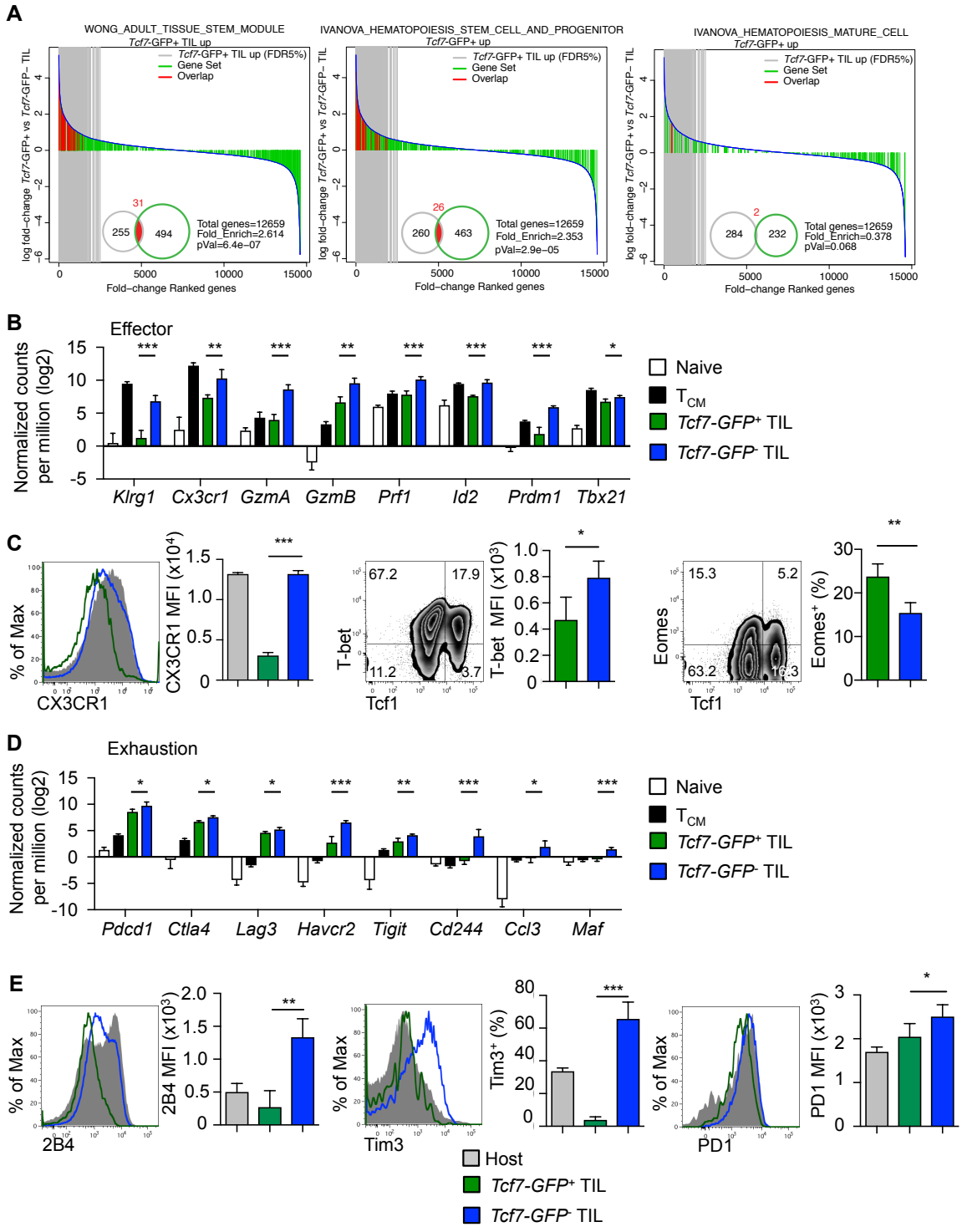

Figure S5. Molecular and phenotypic characterization of Tcf1$^+$ PD1$^+$ TIL. Related to Figure 6.
(**A**) Over-representation analysis shows that genes upregulated in *Tcf7*-GFP$^+$ TIL significantly overlap with those upregulated in adult tissue stem cells (Wong et al., 2008) and hematopoietic stem cells and progenitors but not in mature haematopoietic cells (Ivanova et al., 2002).
(**B-E**) Expression of selected genes associated with effector differentiation and exhaustion in TIL subsets. (**B, D**) The bar graphs show the expression of selected genes associated with (**B**) effector differentiation and (**D**) exhaustion by naive P14 cells (open), T_{CM} (black fill), *Tcf7*-GFP$^+$ TIL (green) and *Tcf7*-GFP$^-$ TIL (blue). (**C, D**) Histogram overlays show the expression of (**C**) effector and (**D**) exhaustion markers in *Tcf7*-GFP$^+$ TIL (green), *Tcf7*-GFP$^-$ TIL (blue) as compared to host CD8 TIL (grey fill). The corresponding bar graphs depict the fraction of positive cells or the mean fluorescence intensity (MFI) of staining.

Data in (**A, B, D**) are derived from RNAseq analysis of n=3-4 independent samples per group. Data in (**C, E**) are representative of at least 2 independent experiments each with n=3-5 mice. Error bars in (**B-E**) are SD. Statistics in (**A**) used hypergeometric test and is based on unpaired t-test in (**C, E**).

Supplemental Figure 6

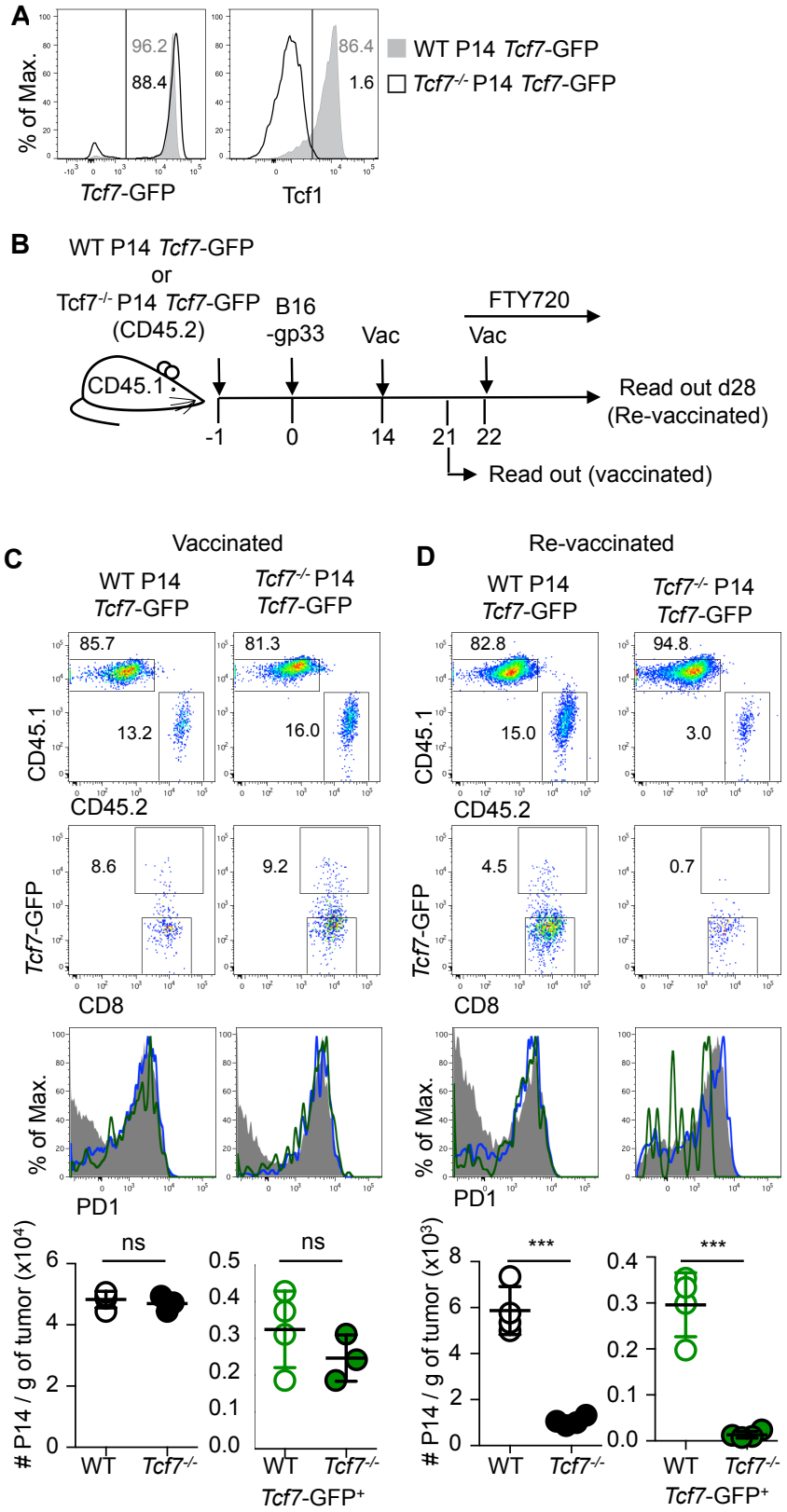

Figure S6. Role of Tcf1 in *Tcf7*-GFP$^+$ precursor cells. Related to Figure 6.
(**A**) WT *Tcf7*-GFP P14 and *Tcf7*$^{-/-}$ Tcf7-GFP P14 cells from naive mice were analyzed for GFP and Tcf1 protein expression. (**B**) Wt *Tcf7*-GFP$^+$ P14 or *Tcf7*$^{-/-}$ *Tcf7*-GFP$^+$ P14 chimeric mice were implanted with B16-gp33 tumor cells and vaccinated when tumors became palpable. TIL were analyzed one week later. A separate group of mice was treated with FTY720 (FTY) to prevent the influx of new T cells into the tumor.

(C, D) Analysis of vaccinated (C) and revaccinated mice (D). Density plots show the abundance of WT *Tcf7*-GFP and *Tcf7*$^{-/-}$ Tcf7-GFP P14 TIL among total CD8 TIL (top) and *Tcf7*-GFP expression among gated P14 cells (Bottom). Histogram overlays depict PD1 expression amongst *Tcf7*-GFP^{+} (green) and *Tcf7*-GFP^{-} P14 TIL (Blue) compared to host CD8 TIL (grey fill). Dot graphs depict the abundance of total WT (open) and *Tcf7*$^{-/-}$ P14 cells (black fill) or WT *Tcf7*-GFP^{+} (green open) and *Tcf7*$^{-/-}$ *Tcf7*-GFP^{+} P14 TIL (green fill) per gram of tumor. Data are representative of 2 independent experiments, each with n=3-5 mice per group. Error bars in (**C, D**) are SD and statistics is based on unpaired t-test.

Supplemental Figure 7

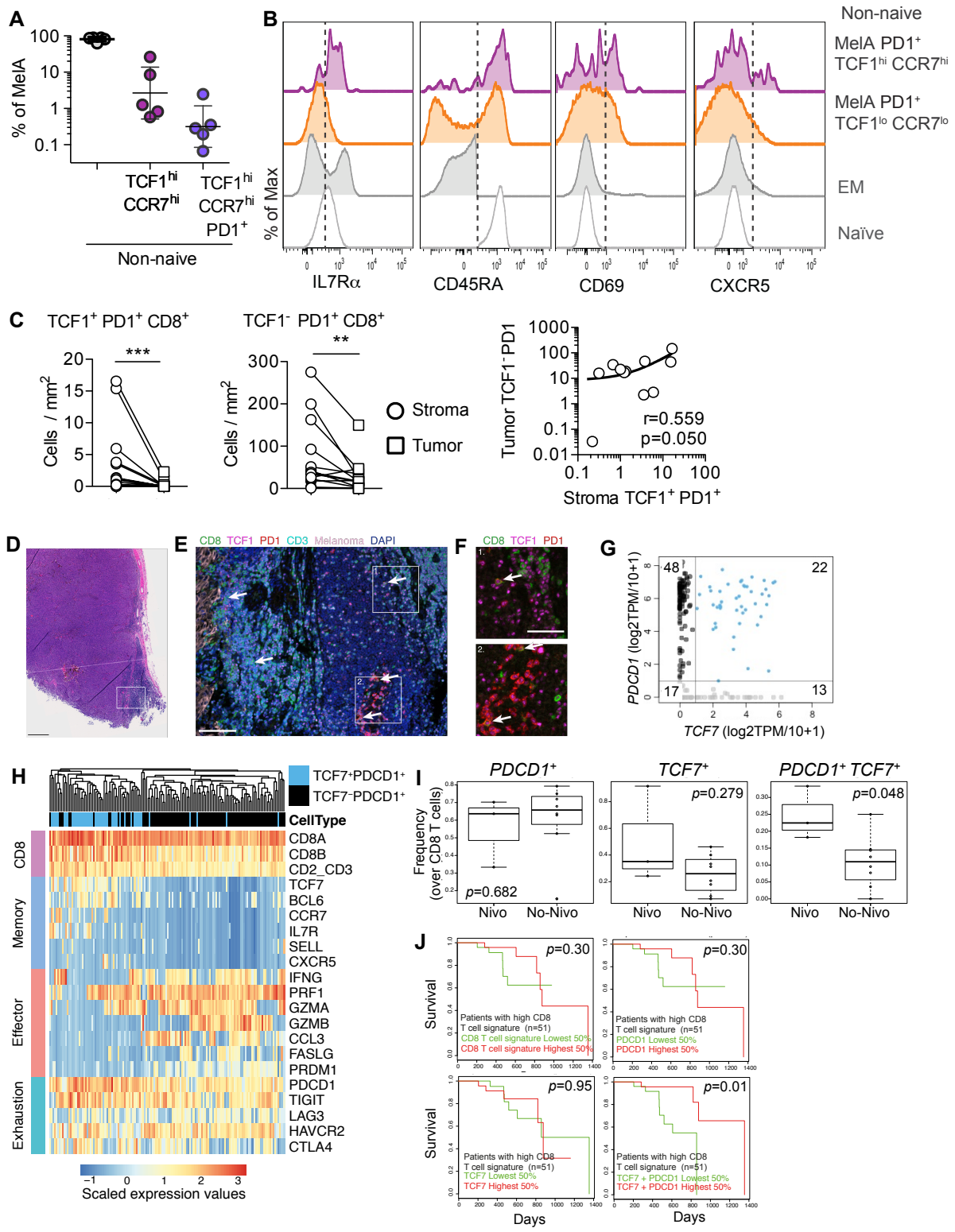

Figure S7. Presence of TCF1$^+$ PD1$^+$ CD8$^+$ T cells in melanoma patients. Related to Figure 7.
(**A, B**) Peripheral blood lymphocytes of melanoma patients (n=5) were analyzed for the presence of non-naive (CD58$^+$ CD95$^+$) MelanA (MelA)-specific CD8 T cells. (**A**) The dot graph depicts the fraction of non-naive MelA CD8 T cells that are Tcf1^{hi} CCR7^{hi} or Tcf1^{hi} CCR7^{hi} PD1$^+$ (n=5 patients, error bars are SD). (**B**) Histograms show the expression of IL7Ra, CD45RA, CD69 and CXCR5 among non-naive CD8 T cells or non-naive MelA CD8 T cell subsets: TCF1^{hi} CCR7^{hi} PD1$^+$ and TCF1^{lo} CCR7^{lo} PD1$^+$. The expression is compared to total effector memory (EM) naive CD8 T cells from the same donor.

(**C**) Quantification of CD8 T cell subsets in multiplex immunostainings of melanoma tissues. Abundance of $TCF1^+$ $PD1^+$ $CD8^+$ T cells (left) and $TCF1^-$ $PD1^+$ $CD8^+$ T cells per per mm^2 (center) in tumor versus stromal area. Correlation between the abundance of $Tcf1^+$ $PD1^+$ and $Tcf1^-$ $PD1^+$ $CD8^+$ T cells in the stroma (right). Data in (**C**) derive from the analysis of n=13 melanoma patients. Statistics is based on paired Wilcoxon test (left and center): *** $p<0.001$, ** $p<0.01$ or non-parametric Spearman correlation.

(D-F) Localization of $TCF1^+$ $PD1^+$ $CD8^+$ T cells in melanoma tissues. **(D)** H&E stain of a melanoma section containing a tertiary lymphoid structure (TLS) as judged by the presence of a dense lymphoid aggregate, with a discrete T cell zone (see **E**). Analysis of the white rectangle highlighted in (**D**) by multiplex immunohistochemistry with Abs to CD8, TCF1, PD1, CD3 and Melanoma markers (HMB-45, MART-1 and Tyrosinase). $TCF1^+$ $PD1^+$ $CD8^+$ T cells, highlighted by arrows, are present in the T cell zone as well as in the putative B cell follicle. The white rectangles depict the areas shown at higher resolution in (**F**). Scale bars represent 500mm in (**D**), 100mm in (**E**) and 50mm in (**F**). TLS were detected in 4 of the 13 patients analyzed.

(G, H) Analysis of melanoma TIL using single cell RNAseq profiling. **(G)** Analysis of $CD8A^+$ melanoma TIL from Mel75 tumor sample for the expression of *TCF7* and *PDCD1* (Tirosh et al., 2016). $TCF7^+$ $PDCD1^+$ $CD8A^+$ TIL (blue), $TCF7^-$ $PDCD1^+$ CD8 TIL (Black). Numbers depict the fraction of $CD8A^+$ T cells in the respective quadrant. (**H**) Expression of genes identifying CD8 T cells (*CD8A, CD8B, CD2, CD3*) and of genes associated with memory, effector differentiation or exhaustion in individual $CD8A^+$ TIL.

(**I**) Box plots show the frequency of CD8 TIL expressing *TCF7 or PDCD1* or co-expressing *TCF7* and *PDCD1* in melanoma patients treated with Ipilimumab and/or Nivolumab versus those that did not receive Nivolumab (No) (Tirosh et al., 2016). Statistics is based on unpaired two-tailed Wilcoxon test.

(**J**) Kaplan Meyer (KM) survival plot in TCGA samples (top 50% most T cell infiltrated samples, excluding lymph node metastases samples), as a function of global T cell infiltration (average expression of *CD8A, CD8B, CD2, CD3G*, *CD3E* and *CD3D*), *TCF7* expression, *PDCD1* expression and combined *TCF7 PDCD1* expression. Indicated *p* values are based on log-rank test.